CrossMark

J. Fluid Mech. (2017), *vol.* 826, *pp.* 335–362. © Cambridge University Press 2017
doi:10.1017/jfm.2017.449

Oscillatory and streaming flow between two spheres due to combined oscillations

Dejuan Kong[1], Anita Penkova[1] and Satwindar Singh Sadhal[1,†]

[1]Department of Aerospace and Mechanical Engineering, University of Southern California, Los Angeles, CA 90089-1453, USA

(Received 7 May 2016; revised 30 March 2017; accepted 23 June 2017;
first published online 3 August 2017)

The flow induced by the combined torsional and transverse oscillations of a sphere with amplitude ratio α and phase difference β in a concentric spherical container is examined. Analytical solutions of the leading-order flow field and shear stress profiles have been obtained. Steady streaming flows are also analysed not only for the case of unrestricted Womersley number $|M|$, but also in the low-frequency ($|M| \ll 1$) and high-frequency ($|M| \gg 1$) limits. At high frequency, the flow field has been divided into three regions: two boundary layers and the outer region. The streaming flow field is determined for the limiting case of the streaming Reynolds number $R_s \ll 1$. The results are compared with those of single torsional or transverse oscillation, and found to match very well. The amplitude ratio α and phase difference β, in determining the streaming, are also discussed. The number and direction of steady streaming recirculation on the r–θ plane depend on value of the amplitude ratio α. The phase difference β plays a dominant role in the azimuthal velocity $u_{1\phi}^{(s)}$ of steady streaming. When β is approximately $(2n+1)\pi/2$, $u_{1\phi}^{(s)}$ vanishes under low-frequency oscillation, while steady streaming has a recirculation on the r–ϕ plane under higher-frequency oscillation.

Key words: acoustics

1. Introduction

Nonlinear effects in oscillatory flow exhibit interesting characteristics, such as streaming that results from oscillatory flows interacting with a solid boundary. Other nonlinear effects can happen with oscillatory disturbances to an otherwise steady flow (Aldridge & Toomre 1969; Busse 2010). In this regard the longitudinal librations of rotating planets have generated interest in the spherical geometry (Sauret *et al.* 2010; Kida 2011; Zhang *et al.* 2013), including a spherical annulus (Noir *et al.* 2009; Calkins *et al.* 2010; Koch *et al.* 2013; Sauret & Le Dizès 2013). For purely oscillation-driven flows, streaming involving drops, bubbles and spherical particles have been the subject of many investigations (Riley 1966; Amin & Riley 1990; Longuet-Higgins 1997, 1998; Zhao, Sadhal & Trinh 1999*a*,*b*; Rednikov, Riley & Sadhal 2003; Repetto, Stocchino & Cafferata 2005; Rednikov *et al.* 2006; Repetto,

† Email address for correspondence: sadhal@usc.edu

https://doi.org/10.1017/jfm.2017.449 Published online by Cambridge University Press

Siggers & Stocchino 2008, 2010; Meskauskas, Repetto & Siggers 2011; Rednikov & Sadhal 2011; Repetto, Siggers & Meskauskas 2014). In terms of torsional motion, Gopinath (1994) did some fundamental work on the problem of the exterior region of a sphere. In particular, he considered combined torsional and transverse oscillations of a sphere. Our work focuses on this type of fundamental analysis and concerns where streaming is generated by both transverse and rotational oscillations of the inner sphere. In the present investigation, the two different types of oscillations are combined with the same angular frequency ω. Due to stronger shear stresses resulting from the interaction of two oscillations as compared to a single type of oscillation, such a case is of particular fundamental interest. It should also be noted that with the same angular frequency ω, the effect of the interaction of two oscillations is greatest, and thus, the magnitude of steady streaming induced is strongest, according to Kelly (1966). In this regard, there is a strong interest in examining the effect of superposed torsional and transverse oscillations in generating the steady streaming with interesting phenomena.

When periodic oscillations are imposed on a body within an incompressible fluid at rest, a steady background appears in addition to the oscillatory flow. This type of non-zero time-averaged flow is referred to as steady streaming. Mathematically, the leading-order solution is oscillatory, and a steady non-zero component exists in the higher-order terms with higher harmonics due to the existence of the nonlinear terms in the Navier–Stokes equation. It was first pointed out by Rayleigh (1884) and later studied by Schlichting (1932). Riley (1998, 2001) reviewed several examples of acoustic streaming, such as the quartz wind introduced by an ultra-high-frequency beam penetrating a fluid, Rayleigh streaming, and torsional oscillations, as well as free surface flow. More recently, Rednikov & Sadhal (2011), Bruus (2012, 2014), Dual *et al.* (2012), Sadhal (2012*a*,*b*,*c*, 2014), Wiklund (2012), Wiklund, Green & Ohlin (2012) and Green, Ohlin & Wiklund (2014) also reviewed several cases of steady streaming. The principles of acoustic streaming have also been presented by Nyborg (1953) and Lighthill (1978).

Many researchers have studied steady streaming generated by oscillations. The steady streaming introduced by torsional oscillations of a spherical cell containing a fluid drop was examined by Zapryanov & Chervenivanova (1981). Three standing vortices in every quadrant between the drop and container, as well as steady streaming inside the drop, were found. In connection with saccadic motion of eyes, Repetto *et al.* (2005, 2008) studied steady streaming in a spherical chamber undergoing periodic torsional oscillation both theoretically and experimentally, and found good agreement between them. They extended the work by considering the effects of viscoelastic fluids (see Repetto *et al.* 2014) as well as that of non-spherical geometry (see Stocchino, Repetto & Cafferata 2007; Repetto *et al.* 2010; Bonfiglio *et al.* 2013) on steady streaming. The flow generated by small-amplitude torsional oscillation of a sphere in a viscous fluid was presented by Riley (1966), Gopinath (1992, 1993) and Mei (1994). These above-mentioned studies provide descriptions of various cases of steady streaming with torsional and transverse oscillations of a solid sphere and spherical container, corresponding to flows in the regions outside a sphere and within a shell. The steady streaming flow generated by superposed small-amplitude oscillations have been examined by Kelly (1966), Panagopoulos, Psillakis & Karahalios (1991) and Riley (1991) for the case of a circular cylinder, and by Gopinath (1994) for the case of a sphere. Longuet-Higgins (1998) studied the streaming induced by a spherical bubble undergoing radial and transverse oscillations simultaneously. The streaming phenomenon has been the subject of many recent investigations in connection with

https://doi.org/10.1017/jfm.2017.449 Published online by Cambridge University Press

manipulation of microparticles with ultrasound (see Jia, Yang & Mei 2012; Muller *et al.* 2013). There has also been interest in microstreaming generated by ultrasound on sessile bubbles (see Wang, Rallabandi & Hilgenfeldt 2013; Rallabandi, Wang & Hilgenfeldt 2014). Rallabandi *et al.* (2014) considered sessile bubbles attached to a wall with the bubble surface oscillating in multiple modes. In the follow-up work (see Rallabandi *et al.* 2015), three-dimensional flow components resulting from confined geometries were presented. However, little has been considered before about flow induced by superposed oscillations for the fluid between two concentric hemispheres, or spheres for that matter.

In § 2, the theoretical analysis is developed to find solutions to the governing equations. The discussion of results follows in § 3.

2. Model formulation and theoretical development

2.1. *Governing equations*

There is a viscous fluid between two concentric spheres, the outer one with radius a and the inner one $R_i < a$. The outer spherical container is held fixed, while the inner sphere is oscillating both torsionally and transversely along the z-axis with a phase lag β' and with an amplitude difference (with α denoting the amplitude ratio). This problem is three-dimensional axisymmetric, and we formulate it in spherical coordinates.

The dimensional Navier–Stokes and continuity equations are

$$\frac{\partial \boldsymbol{u}^*}{\partial t^*} + \boldsymbol{u}^* \cdot \boldsymbol{\nabla}^* \boldsymbol{u}^* = -\frac{1}{\rho}\boldsymbol{\nabla}^* p^* + \nu \boldsymbol{\nabla}^{*2} \boldsymbol{u}^*, \quad \boldsymbol{\nabla}^* \cdot \boldsymbol{u}^* = 0, \tag{2.1a,b}$$

with the boundary conditions,

$$\left.\begin{aligned} &u_r^* = U_0 \sin \omega t^* \cos\theta, \quad u_\theta^* = -U_0 \sin \omega t^* \sin\theta, \\ \text{and} \quad &u_\phi^* = \alpha U_0 \sin[\omega(t^* + \beta')] \sin\theta \quad \text{at } r^* = R_i, \end{aligned}\right\} \tag{2.2a}$$

$$u_r^* = u_\theta^* = u_\phi^* = 0 \quad \text{at } r^* = a. \tag{2.2b}$$

Here, the boundary conditions (2.2*a*) are based on transverse oscillations along, and rotational oscillations about, the z-axis.

The stream function, ψ^*, and angular circulation, Ω^*, related to the velocity components are introduced as

$$u_r^* = -\frac{1}{r^{*2}}\frac{\partial \psi^*}{\partial \mu}, \quad u_\theta^* = -\frac{(1-\mu^2)^{-1/2}}{r^*}\frac{\partial \psi^*}{\partial r^*}, \quad u_\phi^* = \frac{\Omega^*}{r^*(1-\mu^2)^{1/2}}, \tag{2.3}$$

where $\mu = \cos\theta$.

With the velocity, time, radial distance, stream function, angular circulation and shear stress scaled with respect to U_0, ω^{-1}, a, $U_0 a^2$, $U_0 a$, $U_0 \mu a^{-1}$ we introduce dimensionless variables,

$$\boldsymbol{u} = \frac{\boldsymbol{u}^*}{U_0}, \quad t = \omega t^*, \quad \psi = \frac{\psi^*}{U_0 a^2}, \quad \Omega = \frac{\Omega^*}{U_0 a}, \quad \boldsymbol{\nabla} = a\boldsymbol{\nabla}^*, \quad \tau = \frac{\tau^* a}{U_0 \mu}. \tag{2.4}$$

The dimensionless governing equations and boundary conditions satisfied by the stream function ψ and angular circulation Ω take the form (Gopinath 1994),

$$\frac{\partial}{\partial t}(\mathrm{D}^2\psi) + \frac{\varepsilon}{r^2}\left[\frac{\partial(\psi, \mathrm{D}^2\psi)}{\partial(r,\mu)} + 2\mathrm{D}^2\psi \mathrm{L}\psi + 2\Omega \mathrm{L}\Omega\right] = \frac{1}{|M|^2}\mathrm{D}^4\psi, \tag{2.5a}$$

https://doi.org/10.1017/jfm.2017.449 Published online by Cambridge University Press

$$\frac{\partial \Omega}{\partial t} + \frac{\varepsilon}{r^2}\left[\frac{\partial(\psi, \Omega)}{\partial(r, \mu)}\right] = \frac{1}{|M|^2}\mathrm{D}^2\Omega, \tag{2.5b}$$

with boundary conditions

$$-\frac{1}{r^2}\frac{\partial \psi}{\partial \mu} = \mu \sin t, \quad -\frac{(1-\mu^2)^{-1/2}}{r}\frac{\partial \psi}{\partial r} = -\sin t(1-\mu^2)^{1/2},$$
$$\text{and} \quad \frac{\Omega}{r(1-\mu^2)^{1/2}} = \alpha \sin(t+\beta)(1-\mu^2)^{1/2} \quad \text{on } r = b, \tag{2.6a}$$
$$\psi = \frac{\partial \psi}{\partial r} = 0, \quad \Omega = 0 \quad \text{on } r = 1, \tag{2.6b}$$

where

$$\mu = \cos\theta, \quad \beta = \omega\beta', \quad \varepsilon = \frac{U_0}{\omega a}, \quad |M|^2 = \frac{\omega a^2}{\nu}, \quad b = \frac{R_i}{a}$$
$$\mathrm{D}^2 = \frac{\partial^2}{\partial r^2} + \frac{1-\mu^2}{r^2}\frac{\partial^2}{\partial \mu^2}, \quad \text{and} \quad \mathrm{L} = \frac{\mu}{1-\mu^2}\frac{\partial}{\partial r} + \frac{1}{r}\frac{\partial}{\partial \mu}. \tag{2.7}$$

2.2. *The leading-order solutions*

We start out with the following perturbation expansion,

$$\psi = \psi_0 + \text{H.O.T.}, \quad \Omega = \Omega_0 + \text{H.O.T.}, \tag{2.8a,b}$$

where H.O.T. means higher-order terms. Upon substitution into the momentum equation (2.5), the leading-order solutions emerge as

$$\frac{\partial}{\partial t}(\mathrm{D}^2\psi_0) = \frac{1}{|M|^2}\mathrm{D}^4\psi_0, \tag{2.9a}$$
$$\frac{\partial \Omega_0}{\partial t} = \frac{1}{|M|^2}\mathrm{D}^2\Omega_0. \tag{2.9b}$$

After some algebra we obtain

$$\begin{aligned}\psi_0 &= \left[A_0 r^2 + \frac{B_0}{r} + C_0\left(\frac{1}{Mr} - 1\right)\mathrm{e}^{Mr} + D_0\left(\frac{1}{Mr} + 1\right)\mathrm{e}^{-Mr}\right](1-\mu^2)\mathrm{e}^{\mathrm{i}t} + \text{c.c.} \\ &= f(r)\mathrm{e}^{\mathrm{i}t}(1-\mu^2) + \text{c.c.}, \end{aligned} \tag{2.10a}$$
$$\begin{aligned}\Omega_0 &= \left[A_0^*\left(\frac{1}{Mr} - 1\right)\mathrm{e}^{Mr} + B_0^*\left(\frac{1}{Mr} + 1\right)\mathrm{e}^{-Mr}\right](1-\mu^2)\mathrm{e}^{\mathrm{i}t} + \text{c.c.} \\ &= g(r)\mathrm{e}^{\mathrm{i}t}(1-\mu^2) + \text{c.c.}, \end{aligned} \tag{2.10b}$$

where

$$M^2 = \mathrm{i}|M|^2, \tag{2.11a}$$

c.c. denotes the complex conjugate, and details of all the coefficients in (2.10) are provided in appendix B.

The dimensionless shear stresses are

$$\begin{aligned}\tau_{0r\theta} = &\left[-\frac{6B_0}{r^4} + C_0\left(-\frac{6}{Mr^4} + \frac{6}{r^3} - \frac{3M}{r^2} + \frac{M^2}{r}\right)\mathrm{e}^{Mr} + D_0\left(-\frac{6}{Mr^4} - \frac{6}{r^3}\right.\right. \\ &\left.\left. - \frac{3M}{r^2} - \frac{M^2}{r}\right)\mathrm{e}^{-Mr}\right](1-\mu^2)^{1/2}\mathrm{e}^{\mathrm{i}t} + \text{c.c.}, \end{aligned} \tag{2.12a}$$

https://doi.org/10.1017/jfm.2017.449 Published online by Cambridge University Press

$$\tau_{0r\phi} = \left[A_0^*\left(-\frac{3}{Mr^3}+\frac{3}{r^2}-\frac{M}{r}\right)\mathrm{e}^{Mr}+B_0^*\left(-\frac{3}{Mr^3}-\frac{3}{r^2}-\frac{M}{r}\right)\mathrm{e}^{-Mr}\right] \times (1-\mu^2)^{1/2}\mathrm{e}^{\mathrm{i}t}+\mathrm{c.c.}, \tag{2.12b}$$

$$\tau_{0\phi\theta} = 0. \tag{2.12c}$$

2.3. *The solutions to order* ε

The variables to order ε are divided into time-independent and time-dependent parts as

$$\psi_1 = \psi_1^{(s)}+\psi_1^{(u)} = \psi_{10}(r,\mu)+\{\psi_{12}(r,\mu)\mathrm{e}^{2\mathrm{i}t}+\mathrm{c.c.}\}, \tag{2.13a}$$

$$\Omega_1 = \Omega_1^{(s)}+\Omega_1^{(u)} = \Omega_{10}(r,\mu)+\{\Omega_{12}(r,\mu)\mathrm{e}^{2\mathrm{i}t}+\mathrm{c.c.}\}, \tag{2.13b}$$

$$\frac{1}{r^2}\left[\frac{\partial(\psi_0,\mathrm{D}^2\psi_0)}{\partial(r,\mu)}+2\mathrm{D}^2\psi_0\mathrm{L}\psi_0+2\Omega_0\mathrm{L}\Omega_0\right] = \mathcal{F}_0+\{\mathcal{F}_2\mathrm{e}^{2\mathrm{i}t}+\mathrm{c.c.}\}, \tag{2.13c}$$

$$\frac{1}{r^2}\left[\frac{\partial(\psi_0,\Omega_0)}{\partial(r,\mu)}\right] = \mathcal{G}_0+\{\mathcal{G}_2\mathrm{e}^{2\mathrm{i}t}+\mathrm{c.c.}\}, \tag{2.13d}$$

where the superscripts (s) and (u) refer to steady and unsteady parts, respectively.

The steady part of the first-order solutions satisfies

$$\mathrm{D}^4\psi_{10} = |M|^2\mathcal{F}_0, \quad \mathrm{D}^2\Omega_{10} = |M|^2\mathcal{G}_0, \tag{2.14a,b}$$

with homogeneous boundary conditions

$$\psi_{10} = \frac{\partial\psi_{10}}{\partial r} = \Omega_{10} = 0 \quad \text{on } r=b, \quad \text{and} \quad \psi_{10} = \frac{\partial\psi_{10}}{\partial r} = \Omega_{10} = 0 \quad \text{on } r=1. \tag{2.15}$$

The steady part of nonlinear terms may be written as

$$\mathcal{F}_0 = \mathcal{F}_{0r}(r)\mu(1-\mu^2), \quad \mathcal{G}_0 = \mathcal{G}_{0r}(r)\mu(1-\mu^2), \tag{2.16a,b}$$

where

$$\mathcal{F}_{0r}(r) = \frac{2}{r^2}[f(r)\overline{f^{(3)}(r)}+\overline{f(r)}f^{(3)}(r)+g(r)\overline{g'(r)}+\overline{g(r)}g'(r)]-\frac{4}{r^3}[f(r)\overline{f''(r)} +\overline{f(r)}f''(r)+2g(r)\overline{g(r)}]-\frac{4}{r^4}[f(r)\overline{f'(r)}+\overline{f(r)}f'(r)]+\frac{32}{r^5}f(r)\overline{f(r)}, \tag{2.17a}$$

$$\mathcal{G}_{0r}(r) = \frac{2}{r^2}[f(r)\overline{g'(r)}+\overline{f(r)}g'(r)-f'(r)\overline{g(r)}-\overline{f'(r)}g(r)]. \tag{2.17b}$$

Next, we express the stream function and angular circulation of steady streaming in forms as

$$\psi_{10} = f_{10}(r)\mu(1-\mu^2), \quad \Omega_{10} = g_{10}(r)\mu(1-\mu^2). \tag{2.18a,b}$$

The resulting differential equations to order ε become

$$\frac{\mathrm{d}^4}{\mathrm{d}r^4}f_{10}(r)-\frac{12}{r^2}\frac{\mathrm{d}^2}{\mathrm{d}r^2}f_{10}(r)+\frac{24}{r^3}\frac{\mathrm{d}}{\mathrm{d}r}f_{10}(r) = |M|^2\mathcal{F}_{0r}(r), \tag{2.19a}$$

$$\frac{\mathrm{d}^2}{\mathrm{d}r^2}g_{10}(r)-\frac{6}{r^2}g_{10}(r) = |M|^2\mathcal{G}_{0r}(r), \tag{2.19b}$$

with homogeneous boundary conditions.

https://doi.org/10.1017/jfm.2017.449 Published online by Cambridge University Press

With the solutions obtained, the velocity can now be expressed as

$$u_{10r} = \left[c_1 r^3 + c_2 r + \frac{c_3}{r^2} + \frac{c_4}{r^4} + H_1(r) r^3 + H_2(r) r + \frac{H_3(r)}{r^2} + \frac{H_4(r)}{r^4}\right](3\mu^2 - 1), \tag{2.20a}$$

$$u_{10\theta} = \left[-5c_1 r^3 - 3c_2 r + \frac{2c_4}{r^4} - 5H_1(r) r^3 - 3H_2(r) r + \frac{2H_4(r)}{r^4}\right]\mu(1-\mu^2)^{1/2}, \tag{2.20b}$$

$$u_{10\phi} = \left[c_5 r^2 + \frac{c_6}{r^3} + H_5(r) r^2 + \frac{H_6(r)}{r^3}\right]\mu(1-\mu^2)^{1/2}. \tag{2.20c}$$

The stream function and angular circulation take the form

$$\psi_{10} = \left[c_1 r^5 + c_2 r^3 + c_3 + \frac{c_4}{r^2} + H_1(r) r^5 + H_2(r) r^3 + H_3(r) + \frac{H_4(r)}{r^2}\right]\mu(1-\mu^2), \tag{2.21a}$$

$$\Omega_{10} = \left[c_5 r^3 + \frac{c_6}{r^2} + H_5(r) r^3 + \frac{H_6(r)}{r^2}\right], \tag{2.21b}$$

with

$$H_1(r) = -\frac{|M|^2}{200}\int_b^r \frac{\mathcal{F}_{0r}(r')}{r'^2}\,\mathrm{d}r', \tag{2.22a}$$

$$H_2(r) = \frac{7|M|^2}{600}\int_b^r \mathcal{F}_{0r}(r')\,\mathrm{d}r', \tag{2.22b}$$

$$H_3(r) = -\frac{7|M|^2}{600}\int_b^r \mathcal{F}_{0r}(r') r'^3\,\mathrm{d}r', \tag{2.22c}$$

$$H_4(r) = \frac{|M|^2}{200}\int_b^r \mathcal{F}_{0r}(r') r'^5\,\mathrm{d}r', \tag{2.22d}$$

$$H_5(r) = \frac{|M|^2}{5}\int_b^r \frac{\mathcal{G}_{0r}(r')}{r'^2}\,\mathrm{d}r', \tag{2.22e}$$

$$H_6(r) = -\frac{|M|^2}{5}\int_b^r \mathcal{G}_{0r}(r') r'^3\,\mathrm{d}r', \tag{2.22f}$$

and determined coefficients (see appendix B).

While these results are for unrestricted $|M|$, they are mathematically complex. A better insight is achieved with some asymptotic analysis. Therefore, the problem is also discussed separately in the low-frequency ($|M|^2 \ll 1$) and the high-frequency ($|M|^2 \gg 1$) limits.

2.4. *The low-frequency limit, $\varepsilon \ll 1 \ll |M|^{-2}$*

For low frequency, the viscous diffusion thickness is larger than the characteristic dimension of the body, which means vorticity diffuses over a much wider region.

We now seek a perturbation solution of the governing equations in the form

$$\psi = \psi_0 + R\psi_1 + R^2\psi_2 + O(R^3), \tag{2.23a}$$

$$\Omega = \Omega_0 + R\Omega_1 + R^2\Omega_2 + O(R^3), \tag{2.23b}$$

https://doi.org/10.1017/jfm.2017.449 Published online by Cambridge University Press

where R is the oscillatory Reynolds number, defined as

$$R = \varepsilon |M|^2 = \frac{U_0 a}{\nu} \ll 1. \tag{2.24}$$

Then, in the limit of $|M| \to 0$, equations (2.10) and (2.12) can be simplified to

$$\psi_0 = \frac{3b}{2\mathrm{i}(1-b)^4(4+7b+4b^2)}\left[-\frac{1}{3}b^2(1-b^3)\frac{1}{r} + (1-b^5)r - \frac{1}{6}(9-5b^2-4b^5)r^2 + \frac{1}{2}(1-b^2)r^4\right](1-\mu^2)\mathrm{e}^{\mathrm{i}t} + \text{c.c.}, \tag{2.25a}$$

$$\Omega_0 = \frac{1}{2\mathrm{i}}\alpha \mathrm{e}^{\mathrm{i}\beta}\frac{b^2}{1-b^3}\left(\frac{1}{r} - r^2\right)(1-\mu^2)\mathrm{e}^{\mathrm{i}t} + \text{c.c.}, \tag{2.25b}$$

$$\tau_{0r\theta} = \frac{3b}{2\mathrm{i}(1-b)^4(4+7b+4b^2)}\left[2b^2(1-b^3)\frac{1}{r^4} - 3(1-b^2)r\right](1-\mu^2)^{1/2}\mathrm{e}^{\mathrm{i}t} + \text{c.c.}, \tag{2.25c}$$

$$\tau_{0r\phi} = -\left(\frac{3\alpha \mathrm{e}^{\mathrm{i}\beta}}{2\mathrm{i}}\right)\left(\frac{b^2}{1-b^3}\right)\frac{1}{r^3}(1-\mu^2)^{1/2}\mathrm{e}^{\mathrm{i}t} + \text{c.c.}, \tag{2.25d}$$

$$\tau_{0\phi\theta} = 0. \tag{2.25e}$$

Next, solutions of $O(R)$ satisfy

$$\mathrm{D}^4\psi_1 = \frac{1}{r^2}\left[\frac{\partial(\psi_0, \mathrm{D}^2\psi_0)}{\partial(r,\mu)} + 2\mathrm{D}^2\psi_0 \mathrm{L}\psi_0 + 2\Omega_0 \mathrm{L}\Omega_0\right] + O(|M|), \tag{2.26a}$$

$$\mathrm{D}^4\Omega_1 = \frac{1}{r^2}\frac{\partial(\psi_0, \Omega_0)}{\partial(r,\mu)} + O(|M|). \tag{2.26b}$$

We can decompose ψ_1 into steady and unsteady parts,

$$\psi_1 = \psi_1^{(s)} + \psi_1^{(u)} = \psi_{10}(r,\mu) + \{\psi_{12}(r,\mu)\mathrm{e}^{2\mathrm{i}t} + \text{c.c.}\}, \tag{2.27a}$$

$$\Omega_1 = \Omega_1^{(s)} + \Omega_1^{(u)} = \Omega_{10}(r,\mu) + \{\Omega_{12}(r,\mu)\mathrm{e}^{2\mathrm{i}t} + \text{c.c.}\}, \tag{2.27b}$$

with boundary conditions

$$-\frac{1}{r^2}\frac{\partial \psi_{1n}}{\partial \mu} = 0, \quad -\frac{(1-\mu^2)^{-1/2}}{r}\frac{\partial \psi_{1n}}{\partial r} = 0, \quad \text{and} \quad \frac{\Omega_{1n}}{r(1-\mu^2)^{1/2}} = 0 \quad \text{on } r = b, \tag{2.28a}$$

$$\psi_{1n} = \frac{\partial \psi_{1n}}{\partial r} = 0, \quad \Omega_{1n} = 0 \quad \text{on } r = 1 \ (n = 1, 2). \tag{2.28b}$$

The solutions for steady streaming are

$$\psi_1^{(s)} = \left\{\left(a_3\frac{1}{r^2} + a_4 r^3 + a_5 r^5 + a_6\right) + \frac{3b^2(1-b^5)}{16(1-b)^8(4+7b+4b^2)^2}\left[2b^2(1-b^3)\frac{1}{r} + 6(1-b^5)r - (9-5b^2-4b^5)r^2 - 3(1-b^2)r^4\right] + \frac{\alpha^2}{16}\left(\frac{b^2}{1-b^3}\right)^2\left(\frac{1}{r} + r^2\right)\right\}\mu(1-\mu^2) + \text{c.c.}, \tag{2.29a}$$

https://doi.org/10.1017/jfm.2017.449 Published online by Cambridge University Press

$$\Omega_1^{(s)} = \left\{\left(a_1\frac{1}{r^2}+a_2r^3\right)+\left(\frac{3\alpha e^{i\beta}}{112}\right)\frac{b^3}{(1-b)^4(1-b^3)(4+7b+4b^2)} \times\left[28(1-b^5)\frac{1}{r}-14(3-b^2-2b^5)+7(7-5b^2-2b^5)r^2 + 4(1-b^2)r^5\right]\right\}\mu(1-\mu^2)+\text{c.c.}, \tag{2.29b}$$

$$u_{1r}^{(s)} = \left\{\left(a_3\frac{1}{r^4}+a_4r+a_5r^3+a_6\frac{1}{r^2}\right)+\frac{3b^2(1-b^5)}{16(1-b)^8(4+7b+4b^2)^2}\left[2b^2(1-b^3)\frac{1}{r^3} +6(1-b^5)\frac{1}{r}-(9-5b^2-4b^5)-3(1-b^2)r^2\right] +\frac{\alpha^2}{16}\left(\frac{b^2}{1-b^3}\right)^2\left(\frac{1}{r^3}+1\right)\right\}(3\mu^2-1)+\text{c.c.}, \tag{2.29c}$$

$$u_{1\theta}^{(s)} = \left\{\left(2a_3\frac{1}{r^4}-3a_4r-5a_5r^3\right)+\frac{3b^2(1-b^5)}{16(1-b)^8(4+7b+4b^2)^2}\left[2b^2(1-b^3)\frac{1}{r^3} -6(1-b^5)\frac{1}{r}+2(9-5b^2-4b^5)+12(1-b^2)r^2\right] +\frac{\alpha^2}{16}\left(\frac{b^2}{1-b^3}\right)^2\left(\frac{1}{r^3}-2\right)\right\}\mu(1-\mu^2)^{1/2}+\text{c.c.}, \tag{2.29d}$$

$$u_{1\phi}^{(s)} = \left\{\left(a_1\frac{1}{r^3}+a_2r^2\right)+\left(\frac{3\alpha e^{i\beta}}{112}\right)\frac{b^3}{(1-b)^4(1-b^3)(4+7b+4b^2)} \times\left[28(1-b^5)\frac{1}{r^2}-14(3-b^2-2b^5)\frac{1}{r}+7(7-5b^2-2b^5)r+4(1-b^2)r^4\right]\right\} \times\mu(1-\mu^2)^{1/2}+\text{c.c.}, \tag{2.29e}$$

with details of the coefficients in appendix B.

2.5. *The high-frequency limit, $\varepsilon \ll 1 \ll |M|^2$*

In this limit, the viscous diffusion thickness is very small. The vorticity is confined to narrow Stokes layers on the two boundaries. The space between the two spheres can be divided into three regions: the inner region around the inner sphere, the inner region around the container, and the outer region which is the bulk of the annular region. We have depicted a schematic of the different regions in figure 1.

2.5.1. *The oscillating field*

First we consider the inner region, which is the boundary layer around the inner sphere. The inner variables with the Stokes layers are scaled as follows:

$$\eta=(r-b)\frac{|M|}{\sqrt{2}} \quad \text{and} \quad \Psi=\psi\frac{|M|}{\sqrt{2}}. \tag{2.30}$$

https://doi.org/10.1017/jfm.2017.449 Published online by Cambridge University Press

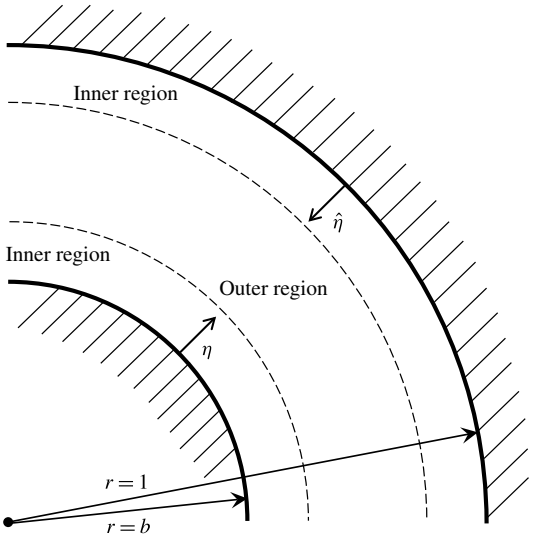


FIGURE 1. A schematic of the streaming flow regions at high frequency.

As a result, the governing equations become

$$\frac{\partial}{\partial t}\left(\frac{\partial^2\Psi}{\partial\eta^2}\right)+\frac{\varepsilon}{b^2}\left[\frac{\partial\left(\Psi,\dfrac{\partial^2\Psi}{\partial\eta^2}\right)}{\partial(\eta,\mu)}+2\frac{\mu}{(1-\mu^2)}\frac{\partial\Psi}{\partial\eta}\frac{\partial^2\Psi}{\partial\eta^2}+2\frac{\mu}{(1-\mu^2)}\Omega\frac{\partial\Omega}{\partial\eta}\right]$$
$$=\frac{1}{2}\frac{\partial^4\Psi}{\partial\eta^4}, \tag{2.31a}$$

$$\frac{\partial\Omega}{\partial t}+\frac{\varepsilon}{b^2}\left[\frac{\partial(\Psi,\Omega)}{\partial(\eta,\mu)}\right]=\frac{1}{2}\frac{\partial^2\Omega}{\partial\eta^2}, \tag{2.31b}$$

with boundary conditions

$$\frac{\partial\Psi}{\partial\mu}=-b^2\frac{|M|}{\sqrt{2}}\mu\sin t,\quad \frac{\partial\Psi}{\partial\eta}=b(1-\mu^2)\sin t,$$
$$\text{and}\quad \Omega=b\alpha(1-\mu^2)\sin(t+\beta)\quad \text{on}\ \ \eta=0. \tag{2.32a}$$

In this case, Ψ and Ω can be expressed as

$$\Psi = \Psi_0+\varepsilon\Psi_1+O(\varepsilon^2), \tag{2.33a}$$
$$\Omega = \Omega_0+\varepsilon\Omega_1+O(\varepsilon^2). \tag{2.33b}$$

We have for the leading order,

$$\frac{\partial}{\partial t}\left(\frac{\partial^2\Psi_0}{\partial\eta^2}\right)=\frac{1}{2}\frac{\partial^4\Psi_0}{\partial\eta^4}, \tag{2.34a}$$
$$\frac{\partial\Omega_0}{\partial t}=\frac{1}{2}\frac{\partial^2\Omega_0}{\partial\eta^2}. \tag{2.34b}$$

https://doi.org/10.1017/jfm.2017.449 Published online by Cambridge University Press

These equations have solutions

$$\Psi_0 = \left\{ a_0 \mathrm{e}^{-(1+\mathrm{i})\eta} + \left[\frac{b}{2\mathrm{i}} + (1+\mathrm{i})a_0 \right] \eta + \frac{|M|}{4\sqrt{2}i} b^2 - a_0 \right\} (1-\mu^2)\mathrm{e}^{\mathrm{i}t} + \text{c.c.}, \quad (2.35a)$$

$$\Omega_0 = \frac{\alpha b}{2\mathrm{i}} (1-\mu^2)\mathrm{e}^{-(1+\mathrm{i})\eta}\mathrm{e}^{\mathrm{i}(t+\beta)} + \text{c.c.} \quad (2.35b)$$

Next, we have two equations for the outer region,

$$\frac{\partial}{\partial t}(\mathrm{D}^2\psi_0) = 0, \quad (2.36a)$$

$$\frac{\partial \Omega_0}{\partial t} = 0. \quad (2.36b)$$

These equations have solutions

$$\psi_0 = \left(a_0^* r^2 + b_0^* \frac{1}{r} \right) (1-\mu^2)\mathrm{e}^{\mathrm{i}t} + \text{c.c.}, \quad (2.37a)$$

$$\Omega_0 = 0. \quad (2.37b)$$

Finally, in the boundary layer on the container, with boundary-layer variables introduced as

$$\hat{\eta} = (1-r)\frac{|M|}{\sqrt{2}} \quad \text{and} \quad \bar{\Psi} = \psi \frac{|M|}{\sqrt{2}}, \quad (2.38)$$

the governing equations become

$$\frac{\partial}{\partial t}\left(\frac{\partial^2 \bar{\Psi}}{\partial \hat{\eta}^2} \right) - \varepsilon \left[\frac{\partial \left(\bar{\Psi}, \dfrac{\partial^2 \bar{\Psi}}{\partial \hat{\eta}^2} \right)}{\partial(\hat{\eta}, \mu)} + 2\frac{\mu}{(1-\mu^2)} \frac{\partial \bar{\Psi}}{\partial \hat{\eta}} \frac{\partial^2 \bar{\Psi}}{\partial \hat{\eta}^2} + 2\frac{\mu}{(1-\mu^2)} \Omega \frac{\partial \Omega}{\partial \hat{\eta}} \right] = \frac{1}{2} \frac{\partial^4 \bar{\Psi}}{\partial \hat{\eta}^4}, \quad (2.39a)$$

$$\frac{\partial \Omega}{\partial t} - \varepsilon \left[\frac{\partial(\bar{\Psi}, \Omega)}{\partial(\hat{\eta}, \mu)} \right] = \frac{1}{2} \frac{\partial^2 \Omega}{\partial \hat{\eta}^2}, \quad (2.39b)$$

with boundary conditions

$$\hat{\eta} = 0, \quad \bar{\Psi} = \frac{\partial \bar{\Psi}}{\partial \hat{\eta}} = \Omega = 0. \quad (2.40)$$

After the perturbation method is applied, solutions to order $O(1)$ in the boundary layer on the container are

$$\bar{\Psi}_0 = d_0[\mathrm{e}^{-(1+\mathrm{i})\hat{\eta}} + (1+\mathrm{i})\hat{\eta} - 1](1-\mu^2)\mathrm{e}^{\mathrm{i}t} + \text{c.c.}, \quad (2.41a)$$

$$\Omega_0 = 0. \quad (2.41b)$$

The coefficients in the solutions of each region are yet undetermined and can be obtained later by matching with the solutions in other regions next to them, according to the requirements

$$\Psi_0|_{\eta \to \infty} = \frac{|M|}{\sqrt{2}} \psi_0|_{r \to b}, \quad (2.42a)$$

https://doi.org/10.1017/jfm.2017.449 Published online by Cambridge University Press

$$\bar{\Psi}_0|_{\hat{\eta}\to\infty} = \frac{|M|}{\sqrt{2}}\psi_0|_{r\to 1}. \tag{2.42b}$$

The matching yields the leading-order solutions as follows. For the outer region,

$$\psi_0 = -\frac{1}{4\mathrm{i}}\left(\frac{b^3}{1-b^3}\right)\left(r^2-\frac{1}{r}\right)(1-\mu^2)\mathrm{e}^{\mathrm{i}t} + \text{c.c.}, \tag{2.43a}$$

$$\Omega_0 = 0. \tag{2.43b}$$

For the inner region around the inner sphere,

$$\Psi_0 = \left\{\frac{3(1+\mathrm{i})}{8}\left(\frac{b}{1-b^3}\right)[\mathrm{e}^{-(1+\mathrm{i})(|M|/\sqrt{2})(r-b)}-1] + \frac{|M|}{4\sqrt{2}}\mathrm{i}\left[\frac{2b^4+b}{1-b^3}(r-b)-b^2\right]\right\} \times (1-\mu^2)\mathrm{e}^{\mathrm{i}t} + \text{c.c.}, \tag{2.44a}$$

$$\Omega_0 = \frac{\alpha b}{2\mathrm{i}}\mathrm{e}^{-(1+\mathrm{i})(|M|/\sqrt{2})(r-b)}(1-\mu^2)\mathrm{e}^{\mathrm{i}(t+\beta)} + \text{c.c.} \tag{2.44b}$$

For the boundary layer around the container,

$$\bar{\psi}_0 = -\frac{3(1+\mathrm{i})}{8}\frac{b^3}{1-b^3}\left[\mathrm{e}^{-(1+\mathrm{i})(|M|/\sqrt{2})(1-r)} + (1+\mathrm{i})\frac{|M|}{\sqrt{2}}(1-r) - 1\right](1-\mu^2)\mathrm{e}^{\mathrm{i}t} + \text{c.c.}, \tag{2.45a}$$

$$\Omega_0 = 0. \tag{2.45b}$$

The composite solution set is

$$\psi_0 = \left[\frac{\sqrt{2}}{|M|}\frac{3(1+\mathrm{i})}{8}\left(\frac{b}{1-b^3}\right)\mathrm{e}^{-(1+\mathrm{i})(|M|/\sqrt{2})(r-b)} - \frac{\sqrt{2}}{|M|}\frac{3(1+\mathrm{i})}{8}\left(\frac{b}{1-b^3}\right)\mathrm{e}^{-(1+\mathrm{i})(|M|/\sqrt{2})(1-r)} - \frac{1}{4\mathrm{i}}\left(\frac{b^3}{1-b^3}\right)\left(r^2-\frac{1}{r}\right)\right](1-\mu^2)\mathrm{e}^{\mathrm{i}t} + \text{c.c.}, \tag{2.46a}$$

$$\Omega_0 = \frac{\alpha b}{2\mathrm{i}}\mathrm{e}^{-(1+\mathrm{i})(|M|/\sqrt{2})(r-b)}(1-\mu^2)\mathrm{e}^{\mathrm{i}(t+\beta)} + \text{c.c.}, \tag{2.46b}$$

and the shear stresses are

$$\tau_{0r\theta} = \left\{\frac{3}{4}\left(\frac{b}{1-b^3}\right)\left[-\frac{2\mathrm{i}}{r^2} - (1+\mathrm{i})\frac{\sqrt{2}}{|M|}\frac{1}{r^3} + (1-\mathrm{i})\frac{|M|}{\sqrt{2}}\frac{1}{r}\right]\mathrm{e}^{-(1+\mathrm{i})(|M|/\sqrt{2})(r-b)} + \frac{3}{4}\left(\frac{b}{1-b^3}\right)\left[-\frac{2\mathrm{i}}{r^2} + (1+\mathrm{i})\frac{\sqrt{2}}{|M|}\frac{1}{r^3} - (1-\mathrm{i})\frac{|M|}{\sqrt{2}}\frac{1}{r}\right]\mathrm{e}^{-(1+\mathrm{i})(|M|/\sqrt{2})(1-r)} - \frac{3}{2\mathrm{i}}\left(\frac{b^3}{1-b^3}\right)\frac{1}{r^4}\right\}(1-\mu^2)^{1/2}\mathrm{e}^{\mathrm{i}t} + \text{c.c.}, \tag{2.47a}$$

$$\tau_{0r\phi} = \frac{\alpha b\mathrm{e}^{\mathrm{i}\beta}}{2\mathrm{i}}\left[-\frac{2}{r^2} - (1+\mathrm{i})\frac{|M|}{\sqrt{2}}\frac{1}{r}\right]\mathrm{e}^{-(1+\mathrm{i})(|M|/\sqrt{2})(r-b)}(1-\mu^2)^{1/2}\mathrm{e}^{\mathrm{i}t} + \text{c.c.}, \tag{2.47b}$$

$$\tau_{0\phi\theta} = 0. \tag{2.47c}$$

https://doi.org/10.1017/jfm.2017.449 Published online by Cambridge University Press

2.5.2. *Steady streaming*

Similarly, to order ε, the streaming is still studied separately in three regions, and then solutions are matched to determine the coefficients in those solutions. Specifically, in the outer region, the steady flow is characterized by the streaming Reynolds number, which is defined as

$$R_s = \frac{U_0^2}{\omega\nu} = \varepsilon^2|M|^2 = \left(\frac{\text{Displacement amplitude of torsional oscillation}}{\text{Stokes-layer thickness}}\right)^2. \quad (2.48)$$

This is not an independent parameter, because it is determined by ε and $|M|$ together. Here, only $R_s \ll 1$ is considered, in which case the governing equation is the Stokes equation.

Then, according to the matching requirement similar to (2.42), solutions in three regions are obtained with all the coefficients determined, and the composite solutions can be written as (see appendix A for procedures)

$$\begin{aligned}\psi_1^{(s)} = &\left\{\frac{\sqrt{2}}{|M|}\left(\frac{2}{b^2}\right)\left[-\frac{3}{4}\left(\frac{\mathrm{i}}{4}\frac{|M|}{\sqrt{2}}b^2 + (1+\mathrm{i})b - \frac{3(5+3\mathrm{i})}{8}\left(\frac{b}{1-b^3}\right)\right)\frac{b}{1-b^3}\right.\right.\\
&\times \mathrm{e}^{-(1+\mathrm{i})(|M|/\sqrt{2})(r-b)} + \frac{1+\mathrm{i}}{32}\left(\frac{9}{4}\left(\frac{b}{1-b^3}\right)^2 - (\alpha b)^2\right)\mathrm{e}^{-2(|M|/\sqrt{2})(r-b)}\\
&\left.\times \frac{3\mathrm{i}}{8}\frac{|M|}{\sqrt{2}}\left(b - \frac{3}{2}\left(\frac{b}{1-b^3}\right)\right)\frac{b}{1-b^3}(r-b)\mathrm{e}^{-(1+\mathrm{i})(|M|/\sqrt{2})(r-b)}\right]\\
&- \frac{\sqrt{2}}{|M|}\left(\frac{9b^6}{8(1-b^3)^2}\right)\left[\frac{1+\mathrm{i}}{8}\mathrm{e}^{-2(|M|/\sqrt{2})(1-r)} + \frac{5+3\mathrm{i}}{2}\mathrm{e}^{-(1+\mathrm{i})(|M|/\sqrt{2})(1-r)}\right.\\
&\left.+\mathrm{i}\frac{|M|}{\sqrt{2}}(1-r)\mathrm{e}^{-(1+\mathrm{i})(|M|/\sqrt{2})(1-r)}\right] + \left(A_3 r^5 + B_3 r^3 + C_3 + \frac{D_3}{r^2}\right)\Bigg\}\\
&\times \mu(1-\mu^2) + \text{c.c.}, \qquad (2.49a)\end{aligned}$$

$$\begin{aligned}\Omega_1^{(s)} = &\left\{\frac{2\alpha\mathrm{e}^{\mathrm{i}\beta}}{b}\left[-\frac{3(1-\mathrm{i})}{16}\left(\frac{b}{1-b^3}\right)\mathrm{e}^{-2(|M|/\sqrt{2})(r-b)} + \frac{1}{4}\left(-\frac{(1-\mathrm{i})}{2}\frac{|M|}{\sqrt{2}}b^2 + 3\mathrm{i}b\right.\right.\right.\\
&\left.\left.- \frac{3(1+3\mathrm{i})}{2}\left(\frac{b}{1-b^3}\right)\right)\mathrm{e}^{-(1+\mathrm{i})(|M|/\sqrt{2})(r-b)}\right.\\
&- \frac{(1-\mathrm{i})}{4}\frac{|M|}{\sqrt{2}}\left(b - \frac{3}{2}\left(\frac{b}{1-b^3}\right)\right)(r-b)\\
&\left.\left.\times \mathrm{e}^{-(1+\mathrm{i})(|M|/\sqrt{2})(r-b)}\right] + A_3^* r^3 + \frac{B_3^*}{r^2}\right\}\mu(1-\mu^2) + \text{c.c.}, \qquad (2.49b)\end{aligned}$$

$$\begin{aligned}u_{1r}^{(s)} = &\left\{\frac{\sqrt{2}}{|M|}\left(\frac{2}{b^2 r^2}\right)\left[-\frac{3}{4}\left(\frac{\mathrm{i}}{4}\frac{|M|}{\sqrt{2}}b^2 + (1+\mathrm{i})b - \frac{3(5+3\mathrm{i})}{8}\left(\frac{b}{1-b^3}\right)\right)\frac{b}{1-b^3}\right.\right.\\
&\times \mathrm{e}^{-(1+\mathrm{i})(|M|/\sqrt{2})(r-b)} + \frac{1+\mathrm{i}}{32}\left(\frac{9}{4}\left(\frac{b}{1-b^3}\right)^2 - (\alpha b)^2\right)\mathrm{e}^{-2(|M|/\sqrt{2})(r-b)}\\
&\left.- \frac{3\mathrm{i}}{8}\frac{|M|}{\sqrt{2}}\left(b - \frac{3}{2}\left(\frac{b}{1-b^3}\right)\right)\frac{b}{1-b^3}(r-b)\mathrm{e}^{-(1+\mathrm{i})(|M|/\sqrt{2})(r-b)}\right]\\
&- \frac{\sqrt{2}}{|M|}\left(\frac{9b^6}{8(1-b^3)^2}\right)\frac{1}{r^2}\left[\frac{1+\mathrm{i}}{8}\mathrm{e}^{-2(|M|/\sqrt{2})(1-r)} + \frac{5+3\mathrm{i}}{2}\mathrm{e}^{-(1+\mathrm{i})(|M|/\sqrt{2})(1-r)}\right.\end{aligned}$$

https://doi.org/10.1017/jfm.2017.449 Published online by Cambridge University Press

$$+\mathrm{i}\frac{|M|}{\sqrt{2}}(1-r)\mathrm{e}^{-(1+\mathrm{i})(|M|/\sqrt{2})(1-r)}\Bigg]+\left(A_3r^3+B_3r+\frac{C_3}{r^2}+\frac{D_3}{r^4}\right)\Bigg\}$$
$$\times(3\mu^2-1)+\text{c.c.}, \tag{2.49c}$$

$$u_{1\theta}^{(s)} = \Bigg\{\frac{2}{b^2r}\Bigg[-\frac{3}{8}\left(-\frac{(1-\mathrm{i})}{2}\frac{|M|}{\sqrt{2}}b^2+3\mathrm{i}b-\frac{3(1+3\mathrm{i})}{2}\left(\frac{b}{1-b^3}\right)\right)\frac{b}{1-b^3}$$
$$\times\mathrm{e}^{-(1+\mathrm{i})(|M|/\sqrt{2})(r-b)}+\frac{1+\mathrm{i}}{16}\left(\frac{9}{4}\left(\frac{b}{1-b^3}\right)^2-(\alpha b)^2\right)\mathrm{e}^{-2(|M|/\sqrt{2})(r-b)}$$
$$+\frac{3(1-\mathrm{i})}{8}\frac{|M|}{\sqrt{2}}\left(b-\frac{3}{2}\left(\frac{b}{1-b^3}\right)\right)\frac{b}{1-b^3}(r-b)\mathrm{e}^{-(1+\mathrm{i})(|M|/\sqrt{2})(r-b)}\Bigg]$$
$$+\frac{9b^6}{8(1-b^3)^2}\frac{1}{r}\Bigg[\frac{1+\mathrm{i}}{4}\mathrm{e}^{-2(|M|/\sqrt{2})(1-r)}+(1+3\mathrm{i})\mathrm{e}^{-(1+\mathrm{i})(|M|/\sqrt{2})(1-r)}$$
$$-(1-\mathrm{i})\frac{|M|}{\sqrt{2}}(1-r)\mathrm{e}^{-(1+\mathrm{i})(|M|/\sqrt{2})(1-r)}\Bigg]+\left(-5A_3r^3-3B_3r+2\frac{D_3}{r^4}\right)\Bigg\}$$
$$\times\mu(1-\mu^2)^{1/2}+\text{c.c.}, \tag{2.49d}$$

$$u_{1\phi}^{(s)} = \Bigg\{\frac{2\alpha\mathrm{e}^{\mathrm{i}\beta}}{br}\Bigg[-\frac{3(1-\mathrm{i})}{16}\left(\frac{b}{1-b^3}\right)\mathrm{e}^{-2(|M|/\sqrt{2})(r-b)}+\frac{1}{4}\left(-\frac{(1-\mathrm{i})}{2}\frac{|M|}{\sqrt{2}}b^2+3\mathrm{i}b\right.$$
$$\left.-\frac{3(1+3\mathrm{i})}{2}\left(\frac{b}{1-b^3}\right)\right)\mathrm{e}^{-(1+\mathrm{i})(|M|/\sqrt{2})(r-b)}$$
$$-\frac{(1-\mathrm{i})}{4}\frac{|M|}{\sqrt{2}}\left(b-\frac{3}{2}\left(\frac{b}{1-b^3}\right)\right)(r-b)$$
$$\times\mathrm{e}^{-(1+\mathrm{i})(|M|/\sqrt{2})(r-b)}\Bigg]+A_3^*r^2+\frac{B_3^*}{r^3}\Bigg\}\mu(1-\mu^2)^{1/2}+\text{c.c.}, \tag{2.49e}$$

and the details of coefficients are provided in appendix B.

3. Results

In figure 2, the leading-order shear stress profiles under different values of the Womersley number $|M|$ are investigated. According to (2.12), transverse oscillations result in the leading-order shear stress $\tau_{0r\theta}$, while torsional oscillations result in $\tau_{0r\phi}$. It means that for combined oscillation, the graphs for leading-order shear stress components are the same as those for transverse or torsional oscillation only, as in our previous work (Kong, Penkova & Sadhal 2015). Also, for both shear stresses, the maximum values can be found on the inner boundary. These maximum values rise with increasing Womersley number $|M|$. As $|M|$ increases to 20, torsional oscillations can lead to shear stress $\tau_{0r\phi}$ mainly close to the inner boundary, while the value of $\tau_{0r\phi}$ is quite small for the outside part of the region. In contrast, influence of transverse oscillation on shear stress $\tau_{0r\theta}$ close to the outer boundary remains the same as $|M|$ rises, as can be seen from the shear stress value on the outer boundary. Especially for low-frequency ($|M|\ll 1$), the shear stress profiles, shown in figure 2(*a*), are similar to those for $|M|=1$ in figure 2(*b*). At low frequency, a reduction of the Womersley number $|M|$ does not cause a significant decrease in shear stress values.

Kong *et al.* (2015) showed that second-order steady streaming, induced by a single transverse or torsional oscillation, is only on the r–θ plane. For transverse oscillation only, the streaming vortex in the first quadrant on the $\phi=0$ plane is clockwise, and

https://doi.org/10.1017/jfm.2017.449 Published online by Cambridge University Press

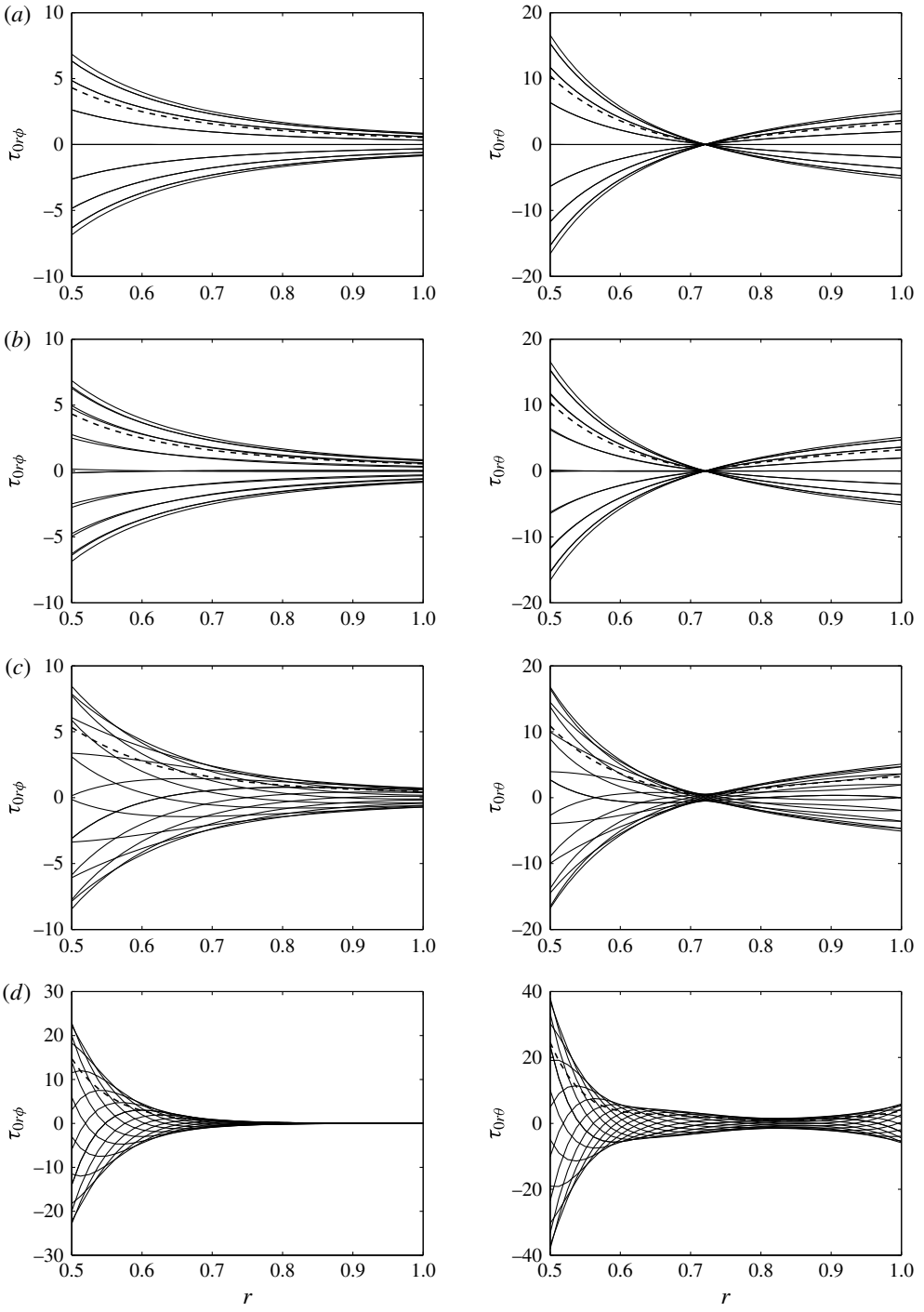


FIGURE 2. Leading-order shear stress profiles on the equatorial plane over one time period with $b = 0.5$, $\alpha = 1$ and $\beta = \pi/4$. The dashed curve shows the time average of absolute shear stress values over one period. (*a*) $|M| \ll 1$, (*b*) $|M| = 1$, (*c*) $|M| = 5$, (*d*) $|M| = 20$.

https://doi.org/10.1017/jfm.2017.449 Published online by Cambridge University Press

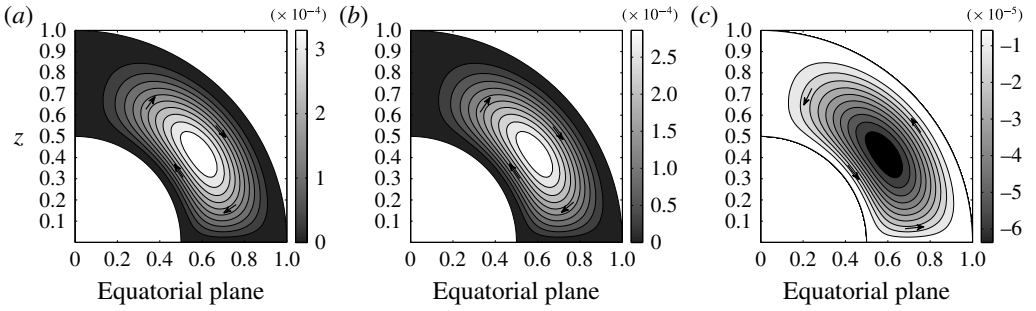


FIGURE 3. The streaming flow pattern on r–θ plane for low frequency under different amplitude ratio with $b = 0.5$. (*a*) $\alpha = 0$, (*b*) $\alpha = 1$, (*c*) $\alpha = 3$.

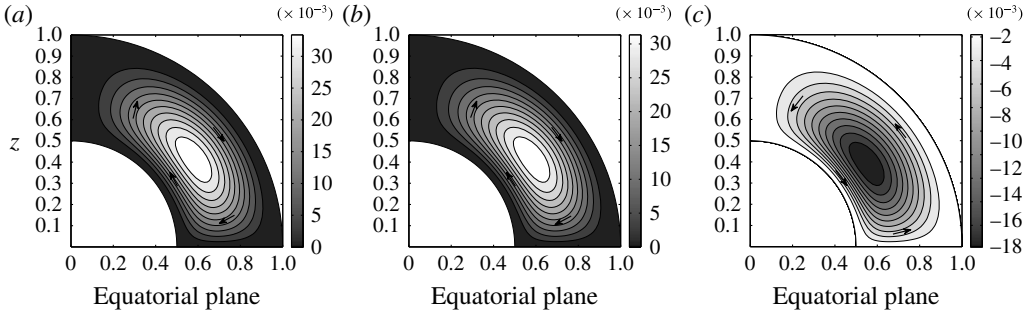


FIGURE 4. The streaming flow pattern on r–θ plane for $|M| = 10$ under different amplitude ratio with $b = 0.5$. (*a*) $\alpha = 0$, (*b*) $\alpha = 1$, (*c*) $\alpha = 5$.

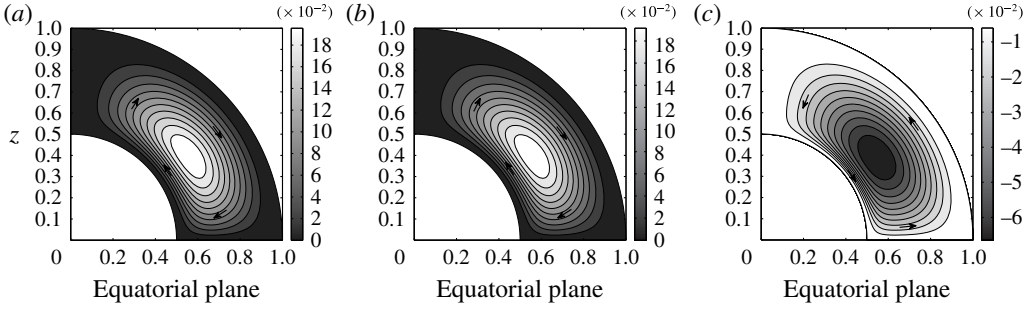


FIGURE 5. The streaming flow pattern on r–θ plane for high frequency ($|M| = 25$) under different amplitude ratio with $b = 0.5$. (*a*) $\alpha = 0$, (*b*) $\alpha = 1$, (*c*) $\alpha = 8$.

counter-clockwise for torsional oscillation only. However, for superposed transverse and torsional oscillations, the azimuthal velocity of steady streaming is non-zero. Steady streaming patterns at low frequency for different values of the amplitude ratio α are plotted in figure 3 (for $|M| = 10$ in figure 4, and for high frequency in figure 5). The vortices of streaming for only transverse oscillation ($\alpha = 0$), shown in figures 3(*a*), 4(*a*) and 5(*a*), are the same as those in Kong *et al.* (2015). As α is increased, the effect of torsional oscillations is enhanced. We take low frequency for example. As the ratio of amplitude α goes up from 1 to 3, the vortex changes

https://doi.org/10.1017/jfm.2017.449 Published online by Cambridge University Press

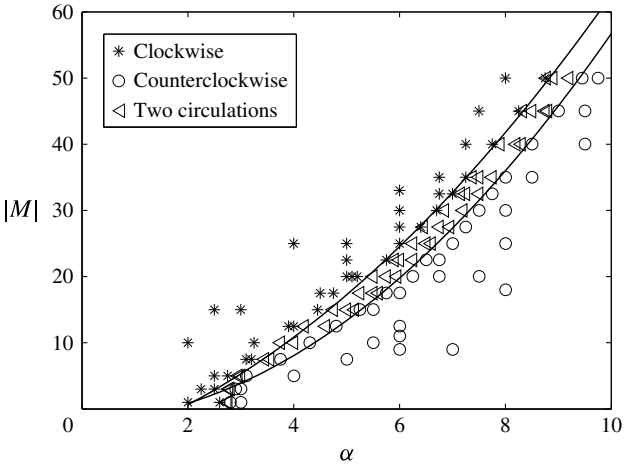


FIGURE 6. Signs of the circulation in the first quadrant on the $\phi = 0$ plane at different $|M|$ and α values.

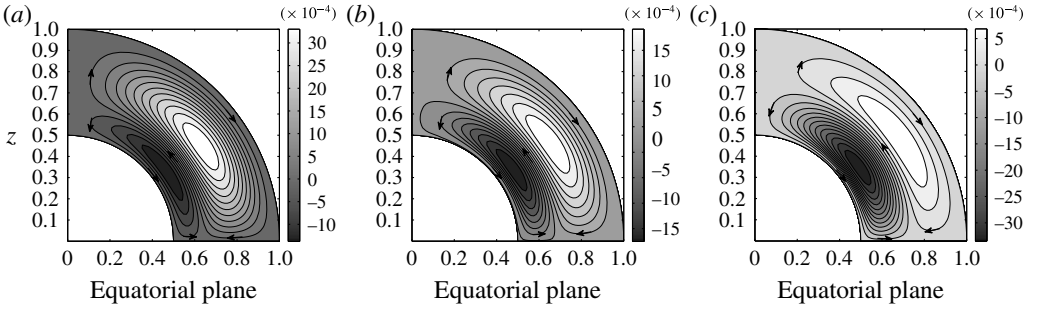


FIGURE 7. Example of the streaming flow pattern change on r–θ plane under different amplitude ratio ($|M| = 10$, $b = 0.5$). (*a*) $\alpha = 3.9$, (*b*) $\alpha = 4.0$, (*c*) $\alpha = 4.1$.

direction from clockwise to counter-clockwise in the first quadrant on the $\phi = 0$ plane. This transition takes place at a value of α between 2 and 3. On the other hand, for $|M| = 10$, torsional oscillation does not play a dominant role until α reaches 5 (figure 4*c*), and 8 for high frequency (figure 5*c*). Signs of the circulation in the first quadrant on the $\phi = 0$ plane at different values of $|M|$ and α are plotted in figure 6.

Corresponding to $|M| = 10$, the transition for flow reversal (figure 4*b*,*c*) is approximately at $\alpha = 4$. The flow field around this transition is detailed in figure 7(*a*–*c*). Some interesting flow patterns have been predicted. With the increase of α, a second vortex with opposite circulation is formed close to the inner boundary (figure 7*a*) around $\alpha = 3.9$. It then grows bigger with increasing α and eventually squeezes out the existing clockwise-directed vortex in the first quadrant on the $\phi = 0$ plane (figure 7*b*,*c*).

For the steady part of first-order azimuthal velocity $u_{1\phi}^{(s)}$, the value is proportional to the oscillation amplitude ratio α according to (2.20), (2.29) and (2.49). So increasing α does not change the direction of the azimuthal velocity, but the value. When compared with the low frequency in figure 8, higher-frequency oscillations can induce more intense streaming. At low frequencies, the azimuthal velocity $u_{1\phi}^{(s)}$ is insignificant.

https://doi.org/10.1017/jfm.2017.449 Published online by Cambridge University Press

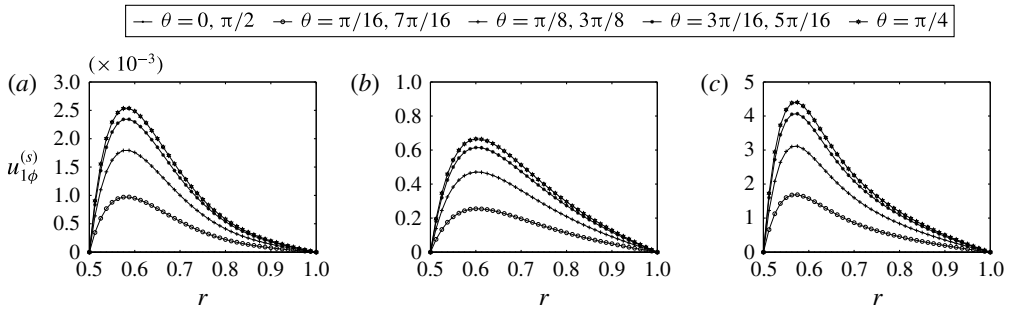


FIGURE 8. Steady part of first order azimuthal velocity profiles with $b = 0.5$, $\alpha = 1$ and $\beta = 0$. (*a*) low frequency, (*b*) $|M| = 10$, (*c*) high frequency ($|M| = 25$).

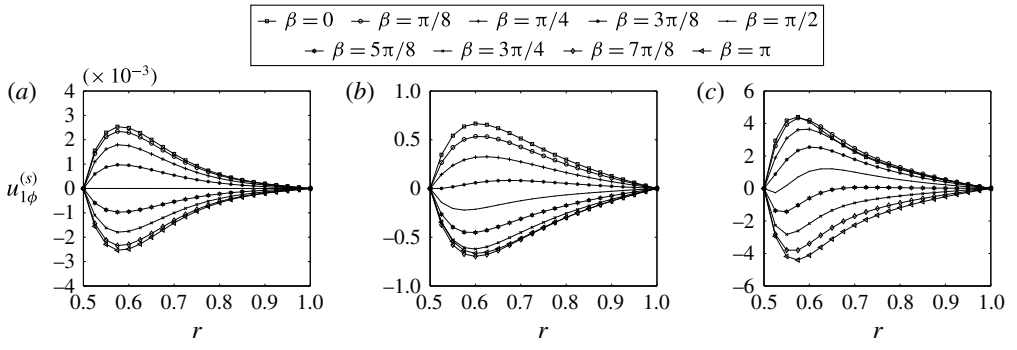


FIGURE 9. Steady part of first-order azimuthal velocity profiles on the plane $\theta = \pi/4$ under different phase difference β with $b = 0.5$, $\alpha = 1$. (*a*) Low frequency, (*b*) $|M| = 10$, (*c*) high frequency ($|M| = 25$).

The phase difference β between the transverse and torsional oscillations does not have an influence on the leading-order solutions, nor on steady streaming on r–θ plane either. However, to order ε, various values of the steady part of the azimuthal velocity are seen with variations of the phase difference β, as shown in figure 9. The magnitude of $u_{1\phi}^{(s)}$ is the greatest for cases in which the phase difference β is approximately $n\pi$, where $n = 0, 1$. For low-frequency oscillation, the azimuthal velocity $u_{1\phi}^{(s)}$ vanishes at a phase difference $\beta = ((2n + 1)\pi)/2$, and no recirculation appears on the r–ϕ plane for any values of phase difference β (figure 9*a*). For higher frequency, take $|M| = 10$ for example (figure 9*b*), the azimuthal velocity $u_{1\phi}^{(s)}$ still exists at a phase difference $\beta = ((2n + 1)\pi)/2$. However, under high-frequency oscillations (figure 9*c*), steady streaming has a recirculation on r–ϕ plane when the phase difference β is approximately in the range from $((2n+1)\pi)/2$ to $((2n+1)\pi + 1/4\pi)/2$.

Since we have results for unrestricted $|M|$ in (2.20), we are in a position to compare these with asymptotic analysis for $|M| \gg 1$. A comparison for various $|M|$ values has been made. Specifically, we have plotted the maximum relative error of the velocity components $u_{1r}^{(s)}$, $u_{1\theta}^{(s)}$, $u_{1\phi}^{(s)}$ between the asymptotic results and the unrestricted $|M|$ ones as a function of r for various values of θ when $|M|$ is between 30 and 100 in figure 10. The plot corresponds to $\alpha = 1$, $\beta = 0$ and $b = 0.5$. The asymptotic results

https://doi.org/10.1017/jfm.2017.449 Published online by Cambridge University Press

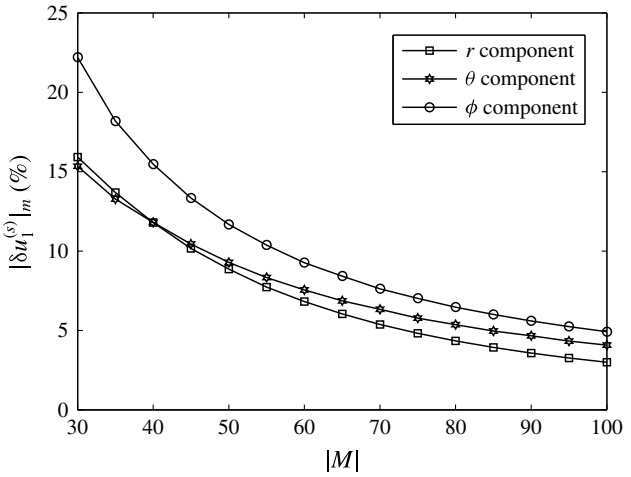


FIGURE 10. Maximum relative error of the steady streaming velocity between asymptotic analysis (2.49) and (2.20) at different $|M|$ values with $b = 0.5$, $\alpha = 1$, $\beta = 0$.

from (2.49) show good agreement with the unrestricted $|M|$ results from (2.20), particularly for $|M| = 100$.

4. Discussion

The present work is concerned with flow induced by combined torsional and transverse oscillations of the inner sphere with a phase lag and amplitude difference in a concentric spherical container. Mathematical analysis has been carried out to obtain the leading-order shear stress distribution and steady streaming characteristics for a large range of Womersley number. Steady streaming is especially discussed for low and high frequency ($|M| \ll 1$ and $|M| \gg 1$).

The leading-order shear stresses $\tau_{0r\phi}$ and $\tau_{0r\theta}$ result from the torsional and transverse oscillations, respectively. These shear stresses $\tau_{0r\phi}$ and $\tau_{0r\theta}$ have a perfect agreement with those induced by single oscillations in our previous work (Kong *et al.* 2015), which was for unrestricted $|M|$ values. The velocity field for steady streaming for the combined oscillations is fully three-dimensional. In particular, the combination produces the ϕ-component of $O(\varepsilon)$ streaming which is absent in the separate torsional and transverse oscillation cases. This is an effect of the nonlinearity of the combination. The amplitude ratio α and phase difference β of two oscillations are important in the determination of steady streaming. On the r–θ plane, since the directions of streaming recirculation are opposite to the single torsional and transverse cases, there is a transition point where the recirculation changes direction when increasing the amplitude ratio α. The α value for the transition point goes up with an increase of Womersley number $|M|$. At high frequency, the effects of transverse oscillation are more obvious compared to those of torsional oscillation. On the other hand, for the azimuthal velocity $u_{1\phi}^{(s)}$ of steady streaming, the amplitude ratio α affects only the value. In addition, the effects of the phase difference β on the azimuthal velocity $u_{1\phi}^{(s)}$ are also discussed. According to the momentum equation (2.5*a*), the r and θ components of the streaming velocity, represented by the streaming flow stream function ψ_{10}, result from interaction of the leading-order stream function ψ_0 with itself, or the leading-order angular circulation Ω_0 with itself. The leading-order

https://doi.org/10.1017/jfm.2017.449 Published online by Cambridge University Press

stream function ψ_0 comes only from transverse oscillation, while the leading-order angular circulation Ω_0 comes only from torsional oscillation. So the phase difference β between the two oscillations does not affect streaming on the r–θ plane. On the other hand, from the momentum equation (2.5*b*), we see that the nonlinear term in the equation of angular circulation Ω, reflecting velocity in the ϕ direction, is the interaction of the stream function ψ and the angular circulation Ω. Thus, the phase difference β only has an influence on the ϕ component of the streaming velocity. When β is in a small range around $((2n+1)\pi)/2$, steady streaming has a recirculation on the r–ϕ plane under high-frequency oscillation, while no recirculation appears and $u_{1\phi}^{(s)}$ vanishes under low-frequency oscillation.

The important contribution here is the analysis of streaming flow within a spherical annulus driven by two oscillatory motions (transverse and torsional) of the inner sphere. As is well known in streaming studies, non-zero mean flow happens at lower orders of perturbation than the case of just one type of oscillation. This phenomenon was illustrated by Kelly (1966) and in the context of the application to spherical geometry in the work of Longuet-Higgins (1998) pertaining to radial pulsation combined with transverse oscillations of a bubble. This problem concerns the exterior of the bubble and the axially symmetric streaming flow does not have a vortical structure. On the other hand, the work of Gopinath (1994) combines torsional and transverse oscillations of a solid sphere leading to fully three-dimensional streaming. Our work builds further on this, and the streaming flow within the annular space is analysed. With both rigid walls, a double boundary-layer structure is found. In addition, there is an interesting vortical structure within the annulus. The double vortical structure takes place in a narrow band on the α–$|M|$ plane, where α is the amplitude ratio between the two oscillations. Outside this band, there is a single vortex structure in each hemisphere.

Appendix A. Derivation of (2.49)

In the boundary layer around the inner sphere, Ψ_1 and Ω_1 satisfy

$$\frac{\partial}{\partial t}\left(\frac{\partial^2\Psi_1}{\partial\eta^2}\right)-\frac{1}{2}\frac{\partial^4\Psi_1}{\partial\eta^4}=-\frac{1}{b^2}\left[\frac{\partial\left(\Psi_0,\dfrac{\partial^2\Psi_0}{\partial\eta^2}\right)}{\partial(\eta,\mu)}+2\frac{\mu}{(1-\mu^2)}\frac{\partial\Psi_0}{\partial\eta}\frac{\partial^2\Psi_0}{\partial\eta^2}\right.$$
$$\left.+2\frac{\mu}{(1-\mu^2)}\Omega_0\frac{\partial\Omega_0}{\partial\eta}\right], \tag{A 1a}$$

$$\frac{\partial\Omega_1}{\partial t}-\frac{1}{2}\frac{\partial^2\Omega_1}{\partial\eta^2}=-\frac{1}{b^2}\frac{\partial(\Psi_0,\Omega_0)}{\partial(\eta,\mu)}, \tag{A 1b}$$

with boundary conditions

$$\frac{\partial\Psi_1}{\partial\mu}=\frac{\partial\Psi_1}{\partial\eta}=\Omega_1=0\quad\text{on }\eta=0. \tag{A 2}$$

The solutions of Ψ_1 and Ω_1 are sought in the form

$$\Psi_1=\Psi_1^{(s)}+\Psi_1^{(u)}=\Psi_{10}(\eta)\mu(1-\mu^2)+\{\Psi_{12}(\eta)\mathrm{e}^{2\mathrm{i}t}\mu(1-\mu^2)+\text{c.c.}\}, \tag{A 3a}$$
$$\Omega_1=\Omega_1^{(s)}+\Omega_1^{(u)}=\Omega_{10}(\eta)\mu(1-\mu^2)+\{\Omega_{12}(\eta)\mathrm{e}^{2\mathrm{i}t}\mu(1-\mu^2)+\text{c.c.}\}. \tag{A 3b}$$

https://doi.org/10.1017/jfm.2017.449 Published online by Cambridge University Press

Steady streaming in the inner region around the inner sphere has solutions

$$\Psi_1^{(s)} = \left\{ \frac{2}{b^2}\left[\frac{1+\mathrm{i}}{32}\left(\frac{9}{4}\left(\frac{b}{1-b^3} \right)^2 - (\alpha b)^2 \right) \mathrm{e}^{-2\eta} - \frac{3}{4}\left(\frac{\mathrm{i}}{4}\frac{|M|}{\sqrt{2}} b^2 + (1+\mathrm{i})b \right.\right.\right.$$
$$\left. - \frac{3(5+3\mathrm{i})}{8}\left(\frac{b}{1-b^3} \right)\right) \frac{b}{1-b^3}\mathrm{e}^{-(1+\mathrm{i})\eta}$$
$$\left. - \frac{3\mathrm{i}}{8}\left(b - \frac{3}{2}\left(\frac{b}{1-b^3} \right)\right) \frac{b}{1-b^3}\eta \mathrm{e}^{-(1+\mathrm{i})\eta}\right]$$
$$\left. + A_1\eta^3 + B_1\eta^2 + C_1\eta + D_1 \right\} \mu(1-\mu^2) + \text{c.c.}, \tag{A 4a}$$

$$\Omega_1^{(s)} = \left\{ \frac{2\alpha \mathrm{e}^{\mathrm{i}\beta}}{b}\left[-\frac{3(1-\mathrm{i})}{16}\frac{b}{1-b^3}\mathrm{e}^{-2\eta} + \frac{1}{4}\left(-\frac{(1-\mathrm{i})}{2}\frac{|M|}{\sqrt{2}} b^2 + 3\mathrm{i}b \right.\right.\right.$$
$$\left. - \frac{3(1+3\mathrm{i})}{2}\left(\frac{b}{1-b^3} \right)\right) \mathrm{e}^{-(1+\mathrm{i})\eta} - \frac{1-\mathrm{i}}{4}\left(b - \frac{3}{2}\left(\frac{b}{1-b^3} \right)\right) \eta \mathrm{e}^{-(1+\mathrm{i})\eta}\right]$$
$$\left. + A_1^*\eta + B_1^* \right\} \mu(1-\mu^2) + \text{c.c.} \tag{A 4b}$$

In the boundary layer on the container, we have

$$\frac{\partial}{\partial t}\left(\frac{\partial^2 \bar{\Psi}_1}{\partial \hat{\eta}^2} \right) - \frac{1}{2}\frac{\partial^4 \bar{\Psi}_1}{\partial \hat{\eta}^4} = \frac{\partial\left(\bar{\Psi}_0, \dfrac{\partial^2 \bar{\Psi}_0}{\partial \hat{\eta}^2} \right)}{\partial(\hat{\eta}, \mu)} + 2\frac{\mu}{(1-\mu^2)}\frac{\partial \bar{\Psi}_0}{\partial \hat{\eta}}\frac{\partial^2 \bar{\Psi}_0}{\partial \hat{\eta}^2}$$
$$+ 2\frac{\mu}{(1-\mu^2)}\Omega_0\frac{\partial \Omega_0}{\partial \hat{\eta}}, \tag{A 5a}$$

$$\frac{\partial \Omega_1}{\partial t} - \frac{1}{2}\frac{\partial^2 \Omega_1}{\partial \hat{\eta}^2} = \frac{\partial(\bar{\Psi}_0, \Omega_0)}{\partial(\hat{\eta}, \mu)}, \tag{A 5b}$$

with boundary conditions

$$\frac{\partial \bar{\Psi}_1}{\partial \mu} = \frac{\partial \bar{\Psi}_1}{\partial \hat{\eta}} = \Omega_1 = 0 \quad \text{on } \hat{\eta} = 0. \tag{A 6}$$

Similarly, we write $\bar{\Psi}_1$ and Ω_1 as

$$\bar{\Psi}_1 = \bar{\Psi}_1^{(s)} + \bar{\Psi}_1^{(u)} = \bar{\Psi}_{10}(\hat{\eta})\mu(1-\mu^2) + \{\bar{\Psi}_{12}(\hat{\eta})\mathrm{e}^{2\mathrm{i}t}\mu(1-\mu^2) + \text{c.c.}\}, \tag{A 7a}$$
$$\Omega_1 = \Omega_1^{(s)} + \Omega_1^{(u)} = \Omega_{10}(\hat{\eta})\mu(1-\mu^2) + \{\Omega_{12}(\hat{\eta})\mathrm{e}^{2\mathrm{i}t}\mu(1-\mu^2) + \text{c.c.}\}. \tag{A 7b}$$

Solutions for steady streaming in the inner region around the container outer shell are

$$\bar{\Psi}_1^{(s)} = \left\{ -\frac{9}{8}\frac{b^6}{(1-b^3)^2}\left[\frac{1+\mathrm{i}}{8}\mathrm{e}^{-2\hat{\eta}} + \frac{5+3\mathrm{i}}{2}\mathrm{e}^{-(1+\mathrm{i})\hat{\eta}} + \mathrm{i}\hat{\eta}\mathrm{e}^{-(1+\mathrm{i})\hat{\eta}}\right]\right.$$
$$\left. + A_2\hat{\eta}^3 + B_2\hat{\eta}^2 + C_2\hat{\eta} + D_2 \right\} \mu(1-\mu^2) + \text{c.c.}, \tag{A 8a}$$

https://doi.org/10.1017/jfm.2017.449 Published online by Cambridge University Press

$$\Omega_1^{(s)} = A_2^* \hat{\eta} \mu (1-\mu^2) + \text{c.c.} \tag{A 8b}$$

All the coefficients need to be determined by boundary conditions and matching with the outer flow.

Accordingly, in the outer region, only $R_s \ll 1$ is considered. We write

$$\psi = \psi_0 + \varepsilon \xi + O(\varepsilon^2), \tag{A 9a}$$

$$\Omega = \Omega_0 + \varepsilon \zeta + O(\varepsilon^2), \tag{A 9b}$$

where ψ_0 and Ω_0 are given before, and ξ and ζ satisfy

$$R_s \frac{\partial}{\partial t}(\mathrm{D}^2 \xi) + \frac{\varepsilon R_s}{r^2}\left[\frac{\partial}{\partial r}(\psi_0 + \varepsilon\xi)\frac{\partial}{\partial \mu}(\mathrm{D}^2\xi) - \frac{\partial}{\partial \mu}(\psi_0 + \varepsilon\xi)\frac{\partial}{\partial r}(\mathrm{D}^2\xi) + 2\mathrm{D}^2\xi \mathrm{L}(\psi_0 + \varepsilon\xi) + 2\varepsilon\zeta \mathrm{L}\zeta\right] = \varepsilon^2 \mathrm{D}^4 \xi, \tag{A 10a}$$

$$R_s \frac{\partial \zeta}{\partial t} + \frac{\varepsilon R_s}{r^2}\left[\frac{\partial}{\partial r}(\psi_0 + \varepsilon\xi)\frac{\partial \zeta}{\partial \mu} - \frac{\partial}{\partial \mu}(\psi_0 + \varepsilon\xi)\frac{\partial \zeta}{\partial r}\right] = \varepsilon^2 \mathrm{D}^2 \zeta, \tag{A 10b}$$

where the operator L is defined in (2.7).

We now expand $\xi(r, \mu, t, \varepsilon)$ and $\zeta(r, \mu, t, \varepsilon)$ in the form

$$\xi = \xi_1 + \varepsilon \xi_2 + \cdots, \tag{A 11a}$$

$$\zeta = \zeta_1 + \varepsilon \zeta_2 + \cdots. \tag{A 11b}$$

The terms of $O(1)$ in (A 9) require that ξ_1 and ζ_1 satisfy

$$\frac{\partial}{\partial t}(\mathrm{D}^2 \xi_1) = 0 \quad \text{and} \quad \frac{\partial \zeta_1}{\partial t} = 0, \tag{A 12a,b}$$

the solutions of which are

$$\xi_1 = F_{10}(r, \mu) + F_{12}(r, \mu)\tilde{T}_1(t) + \text{c.c.} \quad \text{and} \quad \zeta_1 = G_{10}(r, \mu) + \text{c.c.}, \tag{A 13a,b}$$

with

$$\mathrm{D}^2 F_{12}(r, \mu) = 0. \tag{A 14}$$

The terms of $O(\varepsilon)$ give the equation for ξ_2 and ζ_2 as

$$\frac{\partial}{\partial t}(\mathrm{D}^2 \xi_2) + \frac{1}{r^2}\left[\frac{\partial \psi_0}{\partial r}\frac{\partial}{\partial \mu}(\mathrm{D}^2\xi_1) - \frac{\partial \psi_0}{\partial \mu}\frac{\partial}{\partial r}(\mathrm{D}^2\xi_1) + 2\mathrm{D}^2\xi_1 \mathrm{L}\psi_0\right] = 0, \tag{A 15a}$$

$$\frac{\partial \zeta_2}{\partial t} + \frac{1}{r^2}\left[\frac{\partial \psi_0}{\partial r}\frac{\partial \zeta_1}{\partial \mu} - \frac{\partial \psi_0}{\partial \mu}\frac{\partial \zeta_1}{\partial r}\right] = 0, \tag{A 15b}$$

for which, once again,

$$\xi_2 = F_{20}(r, \mu) + F_{22}(r, \mu)\tilde{T}_2(t) + \text{c.c.} \quad \text{and} \quad \zeta_2 = G_{20}(r, \mu) + G_{22}(r, \mu)\tilde{T}_2^*(t) + \text{c.c.} \tag{A 16a,b}$$

Since in (A 15), $\mathrm{D}^2\xi_1$ is independent of t from (A 12), and $\psi_0 \propto \mathrm{e}^{\mathrm{i}t}$ from (2.43), we can write ξ_2 in the form

$$\xi_2 = F_{20}(r, \mu) + F_{22}(r, \mu)\mathrm{e}^{\mathrm{i}t} + \text{c.c.} \tag{A 17}$$

https://doi.org/10.1017/jfm.2017.449 Published online by Cambridge University Press

Similarly, for ζ_2, we have

$$\zeta_2 = G_{20}(r,\mu) + G_{22}(r,\mu)\mathrm{e}^{\mathrm{i}t} + \text{c.c.} \tag{A 18}$$

Then the equations for ξ_3 and ζ_3, obtained from the $O(\varepsilon^2)$ terms are

$$R_s\frac{\partial}{\partial t}(\mathrm{D}^2\xi_3) + \frac{R_s}{r^2}\left[\frac{\partial\psi_0}{\partial r}\frac{\partial}{\partial\mu}(\mathrm{D}^2\xi_2) - \frac{\partial\psi_0}{\partial\mu}\frac{\partial}{\partial r}(\mathrm{D}^2\xi_2) + 2\mathrm{D}^2\xi_2\mathrm{L}\psi_0\right]$$
$$+\frac{R_s}{r^2}\left[\frac{\partial\xi_1}{\partial r}\frac{\partial}{\partial\mu}(\mathrm{D}^2\xi_1) - \frac{\partial\xi_1}{\partial\mu}\frac{\partial}{\partial r}(\mathrm{D}^2\xi_1) + 2\mathrm{D}^2\xi_1\mathrm{L}\xi_1 + 2\zeta_1\mathrm{L}\zeta_1\right] = \mathrm{D}^4\xi_1, \tag{A 19a}$$

$$R_s\frac{\partial\zeta_3}{\partial t} + \frac{R_s}{r^2}\left[\frac{\partial\psi_0}{\partial r}\frac{\partial\zeta_2}{\partial\mu} - \frac{\partial\psi_0}{\partial\mu}\frac{\partial\zeta_2}{\partial r}\right] + \frac{R_s}{r^2}\left[\frac{\partial\xi_1}{\partial r}\frac{\partial\zeta_1}{\partial\mu} - \frac{\partial\xi_1}{\partial\mu}\frac{\partial\zeta_1}{\partial r}\right] = \mathrm{D}^2\zeta_1. \tag{A 19b}$$

We can conclude that $(\partial/\partial t)(D^2\xi_3)$ contains no steady part. Otherwise, ξ_3 would contain terms of $O(t)$, which would lead to unbounded growth in time, according to Rosenblat (1959). It is similar for $\partial\zeta_3/\partial t$.

Because the second terms of (A 19) are in proportion to $\sin t\cos t$, they have no steady part. We may equate the time-independent parts of the $O(\varepsilon^2)$ equations, to get for the steady part

$$\frac{R_s}{r^2}\left[\frac{\partial F_{10}}{\partial r}\frac{\partial}{\partial\mu}(\mathrm{D}^2F_{10}) - \frac{\partial F_{10}}{\partial\mu}\frac{\partial}{\partial r}(\mathrm{D}^2F_{10}) + 2\mathrm{D}^2F_{10}\mathrm{L}F_{10} + 2G_{10}\mathrm{L}G_{10}\right] = \mathrm{D}^4F_{10}, \tag{A 20a}$$

$$\frac{R_s}{r^2}\left[\frac{\partial F_{10}}{\partial r}\frac{\partial G_{10}}{\partial\mu} - \frac{\partial F_{10}}{\partial\mu}\frac{\partial G_{10}}{\partial r}\right] = \mathrm{D}^2G_{10}. \tag{A 20b}$$

Now consider the streaming Reynolds number $R_s \ll 1$ in (A 19) resulting in Stokes-like steady flow, i.e.

$$\mathrm{D}^4F_{10} = 0 \quad \text{and} \quad \mathrm{D}^2G_{10} = 0. \tag{A 21a,b}$$

The appropriate form of solutions should be

$$F_{10}(r,\mu) = \left(A_3r^5 + B_3r^3 + C_3 + \frac{D_3}{r^2}\right)\mu(1-\mu^2), \tag{A 22a}$$

$$G_{10}(r,\mu) = \left(A_3^*r^3 + \frac{B_3^*}{r^2}\right)\mu(1-\mu^2). \tag{A 22b}$$

Steady streaming in the outer region is given by

$$\xi_1^{(s)} = \left(A_3r^5 + B_3r^3 + C_3 + \frac{D_3}{r^2}\right)\mu(1-\mu^2) + \text{c.c.}, \tag{A 23a}$$

$$\zeta_1^{(s)} = \left(A_3^*r^3 + \frac{B_3^*}{r^2}\right)\mu(1-\mu^2) + \text{c.c.} \tag{A 23b}$$

Working through the above derivation, we finally obtained (2.49). More details of the procedures in this section can be found in the work by Riley (1966).

https://doi.org/10.1017/jfm.2017.449 Published online by Cambridge University Press

Appendix B. Coefficients in (2.10), (2.20), (2.29) and (2.49)

Values of the coefficients are provided in this section. The coefficients in (2.10) are given by

$$EA_0 = -\frac{1}{4\mathrm{i}}[\mathrm{e}^{M(1-b)}(3+3Mb+M^2b^2)-\mathrm{e}^{M(b-1)}(3-3Mb+M^2b^2)-6M], \quad \text{(B 1}a\text{)}$$

$$EB_0 = \frac{1}{4\mathrm{i}}\left[\mathrm{e}^{M(1-b)}\left(\frac{3}{M}+3b+Mb^2\right)\left(\frac{3}{M}-3+M\right)\right.$$
$$\left.-\mathrm{e}^{M(b-1)}\left(\frac{3}{M}-3b+Mb^2\right)\left(\frac{3}{M}+3+M\right)\right], \quad \text{(B 1}b\text{)}$$

$$EC_0 = -\frac{1}{4\mathrm{i}}\left[\mathrm{e}^{-Mb}\left(\frac{9}{M}+9b+3Mb^2\right)-\mathrm{e}^{-M}\left(\frac{9}{M}+9+3M\right)\right], \quad \text{(B 1}c\text{)}$$

$$ED_0 = \frac{1}{4\mathrm{i}}\left[\mathrm{e}^{Mb}\left(\frac{9}{M}-9b+3Mb^2\right)-\mathrm{e}^{M}\left(\frac{9}{M}-9+3M\right)\right], \quad \text{(B 1}d\text{)}$$

$$E = 12M+\mathrm{e}^{M(1-b)}\left[3\left(\frac{1}{b}-1\right)-3M\left(\frac{1}{b}+b\right)+M^2\left(\frac{1}{b}-b^2\right)\right]$$
$$-\mathrm{e}^{M(b-1)}\left[3\left(\frac{1}{b}-1\right)+3M\left(\frac{1}{b}+b\right)+M^2\left(\frac{1}{b}-b^2\right)\right], \quad \text{(B 1}e\text{)}$$

$$E^*A_0^* = -\frac{1}{2\mathrm{i}}\alpha\mathrm{e}^{\mathrm{i}\beta}\mathrm{e}^{-M}\left(\frac{1}{M}+1\right), \quad \text{(B 1}f\text{)}$$

$$E^*B_0^* = \frac{1}{2\mathrm{i}}\alpha\mathrm{e}^{\mathrm{i}\beta}\mathrm{e}^{M}\left(\frac{1}{M}-1\right), \quad \text{(B 1}g\text{)}$$

$$E^* = \left(\frac{1}{M}-1\right)\left(\frac{1}{Mb^2}+\frac{1}{b}\right)\mathrm{e}^{M(1-b)}-\left(\frac{1}{M}+1\right)\left(\frac{1}{Mb^2}-\frac{1}{b}\right)\mathrm{e}^{M(b-1)}. \quad \text{(B 1}h\text{)}$$

The coefficients of (2.20) are

$$c_1D^* = H_1(b)(-21b^2+25b^4-4b^7)+H_2(b)(-15+15b^2)+H_3(b)\left(-\frac{6}{b^3}+6b^2\right)$$
$$+H_4(b)\left(-\frac{10}{b^3}+10\right)+H_1(1)\left(-\frac{4}{b^3}+25-21b^2\right)+H_2(1)(15-15b^2)$$
$$+H_3(1)\left(\frac{6}{b^3}-6b^2\right)+H_4(1)\left(\frac{10}{b^3}-10\right), \quad \text{(B 2}a\text{)}$$

$$c_2D^* = H_1(b)(35b^2-35b^4)+H_2(b)(25-21b^2-4b^7)+H_3(b)\left(\frac{10}{b^3}-10b^4\right)$$
$$+H_4(b)\left(\frac{14}{b^3}-14b^2\right)+H_1(1)(-35b^2+35b^4)$$
$$+H_2(1)\left(-\frac{4}{b^3}-21b^2+25b^4\right)+H_3(1)\left(-\frac{10}{b^3}+10b^4\right)$$
$$+H_4(1)\left(-\frac{14}{b^3}+14b^2\right), \quad \text{(B 2}b\text{)}$$

$$c_3D^* = H_1(b)(-14b^2+14b^7)+H_2(b)(-10+10b^7)+H_3(b)\left(-\frac{4}{b^3}-21b^2+25b^4\right)$$

https://doi.org/10.1017/jfm.2017.449 Published online by Cambridge University Press

$$+H_4(b)(-35+35b^2)+H_1(1)(14b^2-14b^7)+H_2(1)(10-10b^7)$$
$$+H_3(1)(25-21b^2-4b^7)+H_4(1)(35-35b^2), \tag{B 2c}$$

$$c_4D^* = H_1(b)(10b^4-10b^7)+H_2(b)(6b^2-6b^7)+H_3(b)(15b^2-15b^4)$$
$$+H_4(b)\left(-\frac{4}{b^3}+25-21b^2\right)+H_1(1)(-10b^4+10b^7)+H_2(1)(-6b^2+6b^7)$$
$$+H_3(1)(-15b^2+15b^4)+H_4(1)(-21b^2+25b^4-4b^7), \tag{B 2d}$$

$$c_5 = \frac{1}{1-b^5}[H_5(b)b^5+H_6(b)-H_5(1)-H_6(1)], \tag{B 2e}$$

$$c_6 = \frac{1}{1-b^5}[-H_5(b)b^5-H_6(b)+H_5(1)b^5+H_6(1)b^5], \tag{B 2f}$$

$$D^* = \frac{4}{b^3}-25+42b^2-25b^4+4b^7. \tag{B 2g}$$

Equation (2.29) has coefficients given by

$$a_1 = -\left(\frac{3\alpha e^{i\beta}}{112}\right)\frac{b^5}{(1-b)^4(1-b^3)(1-b^5)(4+7b+4b^2)}\left(\frac{28}{b}-42+63b^2-39b^3\right.$$
$$\left.-63b^4+57b^5-18b^7+14b^8\right), \tag{B 3a}$$

$$a_2 = -\left(\frac{3\alpha e^{i\beta}}{112}\right)\frac{b^5}{(1-b)^4(1-b^3)(1-b^5)(4+7b+4b^2)}\left(\frac{39}{b^2}-\frac{28}{b}+17-63b^2\right.$$
$$\left.-14b^3+63b^4-32b^5+18b^7\right), \tag{B 3b}$$

$$a_3 = \frac{1}{4b^7-25b^4+42b^2-25+\frac{4}{b^3}}[T_1(-15b^4+15b^2)+T_2(-2b^7+5b^4-3b^2)$$
$$+T_3(15b^4-15b^2)+T_4(-3b^5+5b^3-2)], \tag{B 3c}$$

$$a_4 = \frac{1}{4b^7-25b^4+42b^2-25+\frac{4}{b^3}}\left[T_1\left(-10b^4+\frac{10}{b^3}\right)+T_2\left(7b^2-5b^4-\frac{2}{b^3}\right)\right.$$
$$\left.+T_3\left(10b^4-\frac{10}{b^3}\right)+T_4\left(-2b^5-\frac{5}{b^2}+7\right)\right], \tag{B 3d}$$

$$a_5 = \frac{1}{4b^7-25b^4+42b^2-25+\frac{4}{b^3}}\left[T_1\left(6b^2-\frac{6}{b^3}\right)+T_2\left(3b^2-5+\frac{2}{b^3}\right)\right.$$
$$\left.+T_3\left(-6b^2+\frac{6}{b^3}\right)+T_4\left(2b^3-5+\frac{3}{b^2}\right)\right], \tag{B 3e}$$

$$a_6 = \frac{1}{4b^7-25b^4+42b^2-25+\frac{4}{b^3}}\left[T_1(4b^7+21b^2-25)+T_2(2b^7-7b^2+5)\right.$$
$$\left.+T_3\left(-25b^4+21b^2+\frac{4}{b^3}\right)+T_4\left(5b^5-7b^3+\frac{2}{b^2}\right)\right] \tag{B 3f}$$

$$T_1 = -\frac{3b^2(1-b^5)}{16(1-b)^8(4+7b+4b^2)^2}(-6+10b^2-4b^5)-\frac{1}{8}\alpha^2\left(\frac{b^2}{1-b^3}\right)^2, \tag{B 3g}$$

https://doi.org/10.1017/jfm.2017.449 Published online by Cambridge University Press

$$T_2 = -\frac{3b^2(1-b^5)}{16(1-b)^8(4+7b+4b^2)^2}(-24+20b^2+4b^5) - \frac{1}{16}\alpha^2\left(\frac{b^2}{1-b^3}\right)^2, \tag{B 3h}$$

$$T_3 = -\frac{3b^2(1-b^5)}{16(1-b)^8(4+7b+4b^2)^2}(8b-9b^2-3b^6+4b^7) - \frac{1}{16}\alpha^2\left(\frac{b^2}{1-b^3}\right)^2\left(\frac{1}{b}+b^2\right), \tag{B 3i}$$

$$T_4 = -\frac{3b^2(1-b^5)}{16(1-b)^8(4+7b+4b^2)^2}(4-18b+6b^5+8b^6) - \frac{1}{16}\alpha^2\left(\frac{b^2}{1-b^3}\right)^2\left(-\frac{1}{b^2}+2b\right). \tag{B 3j}$$

Finally, the coefficients of (2.49) are given by

$$A_3 = \frac{1}{4b^7-25b^4+42b^2-25+\frac{4}{b^3}}\left[C_1\left(2b^3-5+\frac{3}{b^2}\right) + D_1\left(-\frac{6\sqrt{2}}{|M|}b^2+\frac{6\sqrt{2}}{|M|}\frac{1}{b^3}\right) + C_2\left(-3b^2+5-\frac{2}{b^3}\right)+D_2\left(\frac{6\sqrt{2}}{|M|}b^2-\frac{6\sqrt{2}}{|M|}\frac{1}{b^3}\right)\right], \tag{B 4a}$$

$$B_3 = \frac{1}{4b^7-25b^4+42b^2-25+\frac{4}{b^3}}\left[C_1\left(-2b^5+7-\frac{5}{b^2}\right) + D_1\left(\frac{10\sqrt{2}}{|M|}b^4-\frac{10\sqrt{2}}{|M|}\frac{1}{b^3}\right) + C_2\left(5b^4-7b^2-\frac{2}{b^3}\right)+D_2\left(-\frac{10\sqrt{2}}{|M|}b^4+\frac{10\sqrt{2}}{|M|}\frac{1}{b^3}\right)\right], \tag{B 4b}$$

$$C_3 = \frac{1}{4b^7-25b^4+42b^2-25+\frac{4}{b^3}}\left[C_1\left(5b^5-7b^3+\frac{2}{b^2}\right) + D_1\left(-\frac{25\sqrt{2}}{|M|}b^4+\frac{21\sqrt{2}}{|M|}b^2+\frac{4\sqrt{2}}{|M|}\frac{1}{b^3}\right)+C_2(-2b^7+7b^2-5) + D_2\left(\frac{4\sqrt{2}}{|M|}b^7+\frac{21\sqrt{2}}{|M|}b^2-\frac{25\sqrt{2}}{|M|}\right)\right], \tag{B 4c}$$

$$D_3 = \frac{1}{4b^7-25b^4+42b^2-25+\frac{4}{b^3}}\left[C_1(-3b^5+5b^3-2) + D_1\left(\frac{15\sqrt{2}}{|M|}b^4-\frac{15\sqrt{2}}{|M|}b^2\right)\right.$$

https://doi.org/10.1017/jfm.2017.449 Published online by Cambridge University Press

$$+ C_2(2b^7 - 5b^4 + 3b^2) + D_2\left(-\frac{15\sqrt{2}}{|M|}b^4 + \frac{15\sqrt{2}}{|M|}b^2\right)\Bigg], \tag{B 4d}$$

$$A_3^* = -\left(\frac{\alpha e^{i\beta}}{2b}\right)\frac{1}{b^3 - \frac{1}{b^2}}\left[-\frac{(1-i)}{2}\frac{|M|}{\sqrt{2}}b^2 + 3ib - \frac{3(3+5i)}{4}\left(\frac{b}{1-b^3}\right)\right], \tag{B 4e}$$

$$B_3^* = \left(\frac{\alpha e^{i\beta}}{2b}\right)\frac{1}{b^3 - \frac{1}{b^2}}\left[-\frac{(1-i)}{2}\frac{|M|}{\sqrt{2}}b^2 + 3ib - \frac{3(3+5i)}{4}\left(\frac{b}{1-b^3}\right)\right], \tag{B 4f}$$

$$C_1 = -\frac{2}{b^2}\left\{-\frac{1+i}{16}\left[\frac{9}{4}\left(\frac{b}{1-b^3}\right)^2 - (\alpha b)^2\right] + \frac{3}{4}\left[-\frac{(1-i)|M|}{4\sqrt{2}}b^2 + \frac{3i}{2}b - \frac{3(1+3i)}{4}\frac{b}{1-b^3}\right]\frac{b}{1-b^3}\right\}, \tag{B 4g}$$

$$D_1 = -\frac{2}{b^2}\left\{\frac{1+i}{32}\left[\frac{9}{4}\left(\frac{b}{1-b^3}\right)^2 - (\alpha b)^2\right] - \frac{3}{4}\left[-\frac{i|M|}{4\sqrt{2}}b^2 + (1+i)b - \frac{3(5+3i)}{8}\frac{b}{1-b^3}\right]\frac{b}{1-b^3}\right\}, \tag{B 4h}$$

$$C_2 = -\frac{9(5+13i)}{32}\frac{b^6}{(1-b^3)^2}, \tag{B 4i}$$

$$D_2 = \frac{9(21+13i)}{64}\frac{b^6}{(1-b^3)^2}. \tag{B 4j}$$

REFERENCES

ALDRIDGE, K. D. & TOOMRE, A. 1969 Axisymmetric inertial oscillations of a fluid in a rotating spherical container. *J. Fluid Mech.* **37** (02), 307–323.

AMIN, N. & RILEY, N. 1990 Streaming from a sphere due to a pulsating source. *J. Fluid Mech.* **210**, 459–473.

BONFIGLIO, A., REPETTO, R., SIGGERS, J. H. & STOCCHINO, A. 2013 Investigation of the motion of a viscous fluid in the vitreous cavity induced by eye rotations and implications for drug delivery. *Phys. Med. Biol.* **58** (6), 1969–1982.

BRUUS, H. 2012 Acoustofluidics 2: perturbation theory and ultrasound resonance modes. *Lab on a Chip* **12** (1), 20–28.

BRUUS, H. 2014 Perturbation theory and ultrasound resonances. In *Microscale Acoustofluidics* (ed. T. Laurell & A. Lenshof), pp. 29–45. Royal Society of Chemistry.

BUSSE, F. H. 2010 Mean zonal flows generated by librations of a rotating spherical cavity. *J. Fluid Mech.* **650**, 505–512.

CALKINS, M. A., NOIR, J., ELDREDGE, J. D. & AURNOU, J. M. 2010 Axisymmetric simulations of libration-driven fluid dynamics in a spherical shell geometry. *Phys. Fluids* **22** (8), 086602.

DUAL, J., HAHN, P., LEIBACHER, I., MÖLLER, D., SCHWARZ, T. & WANG, J. 2012 Acoustofluidics 19: ultrasonic microrobotics in cavities: devices and numerical simulation. *Lab on a Chip* **12** (20), 4010–4021.

GOPINATH, A. 1992 Convective heat transfer in acoustic streaming flows. PhD thesis, University of California, Los Angeles.

GOPINATH, A. 1993 Steady streaming due to small-amplitude torsional oscillations of a sphere in a viscous fluid. *Q. J. Mech. Appl. Maths* **46** (3), 501–520.

https://doi.org/10.1017/jfm.2017.449 Published online by Cambridge University Press

GOPINATH, A. 1994 Steady streaming due to small-amplitude superposed oscillations of a sphere in a viscous fluid. *Q. J. Mech. Appl. Maths* **47** (3), 461–480.

GREEN, R., OHLIN, M. & WIKLUND, M. 2014 Applications of acoustic streaming. In *Microscale Acoustofluidics* (ed. T. Laurell & A. Lenshof), pp. 312–336. Royal Society of Chemistry.

JIA, K., YANG, K. & MEI, D. 2012 Quantitative trap and long range transportation of micro-particles by using phase controllable acoustic wave. *J. Appl. Phys.* **112** (5), 054908.

KELLY, R. E. 1966 Streaming effects associated with doubly oscillating cylinders. *Q. J. Mech. Appl. Maths* **19** (4), 473–484.

KIDA, S. 2011 Steady flow in a rapidly rotating sphere with weak precession. *J. Fluid Mech.* **680**, 150–193.

KOCH, S., HARLANDER, U., EGBERS, C. & HOLLERBACH, R. 2013 Inertial waves in a spherical shell induced by librations of the inner sphere: experimental and numerical results. *Fluid Dyn. Res.* **45** (3), 035504.

KONG, D., PENKOVA, A. & SADHAL, S. S. 2015 Oscillatory flow between two hemispheres for shearing protein solution. *Trans. ASME J. Fluids Engng* **137** (10), 101201.

LIGHTHILL, J. 1978 Acoustic streaming. *J. Sound Vib.* **61** (3), 391–418.

LONGUET-HIGGINS, M. S. 1997 Particle drift near an oscillating bubble. In *Proc. R. Soc. Lond. Series A: Math. Phys. Eng. Sci.*, vol. 453, pp. 1551–1568. The Royal Society.

LONGUET-HIGGINS, M. S. 1998 Viscous streaming from an oscillating spherical bubble. In *Proc. R. Soc. Lond. Series A: Math. Phys. Eng. Sci.*, vol. 454, pp. 725–742. The Royal Society.

MEI, R. 1994 Flow due to an oscillating sphere and an expression for unsteady drag on the sphere at finite Reynolds number. *J. Fluid Mech.* **270**, 133–174.

MESKAUSKAS, J., REPETTO, R. & SIGGERS, J. H. 2011 Oscillatory motion of a viscoelastic fluid within a spherical cavity. *J. Fluid Mech.* **685**, 1–22.

MULLER, P. B., ROSSI, M., MARÍN, Á. G., BARNKOB, R., AUGUSTSSON, P., LAURELL, T., KAEHLER, C. J. & BRUUS, H. 2013 Ultrasound-induced acoustophoretic motion of microparticles in three dimensions. *Phys. Rev.* E **88** (2), 023006.

NOIR, J., HEMMERLIN, F., WICHT, J., BACA, S. M. & AURNOU, J. M. 2009 An experimental and numerical study of librationally driven flow in planetary cores and subsurface oceans. *Phys. Earth Planet. Inter.* **173** (1), 141–152.

NYBORG, W. L. 1953 Acoustic streaming due to attenuated plane waves. *J. Acoust. Soc. Am.* **25** (1), 68–75.

PANAGOPOULOS, A. A., PSILLAKIS, Z. M. & KARAHALIOS, G. T. 1991 Steady streaming induced by a cylinder performing transverse and torsional oscillations. *Phys. Fluids* A **3** (5), 782–792.

RALLABANDI, B., MARIN, A., ROSSI, M., KÄHLER, C. J. & HILGENFELDT, S. 2015 Three-dimensional streaming flow in confined geometries. *J. Fluid Mech.* **777**, 408–429.

RALLABANDI, B., WANG, C. & HILGENFELDT, S. 2014 Two-dimensional streaming flows driven by sessile semicylindrical microbubbles. *J. Fluid Mech.* **739**, 57–71.

RAYLEIGH, L. 1884 On the circulation of air observed in kundt's tubes, and on some allied acoustical problems. *Phil. Trans. R. Soc. Lond.* A **175**, 1–21.

REDNIKOV, A. Y., RILEY, N. & SADHAL, S. S. 2003 The behaviour of a particle in orthogonal acoustic fields. *J. Fluid Mech.* **486**, 1–20.

REDNIKOV, A. Y. & SADHAL, S. S. 2011 Acoustic/steady streaming from a motionless boundary and related phenomena: generalized treatment of the inner streaming and examples. *J. Fluid Mech.* **667**, 426–462.

REDNIKOV, A. Y., ZHAO, H., SADHAL, S. S. & TRINH, E. H. 2006 Steady streaming around a spherical drop displaced from the velocity antinode in an acoustic levitation field. *Q. J. Mech. Appl. Maths* **59** (3), 377–397.

REPETTO, R., SIGGERS, J. H. & MESKAUSKAS, J. 2014 Steady streaming of a viscoelastic fluid within a periodically rotating sphere. *J. Fluid Mech.* **761**, 329–347.

REPETTO, R., SIGGERS, J. H. & STOCCHINO, A. 2008 Steady streaming within a periodically rotating sphere. *J. Fluid Mech.* **608**, 71–80.

https://doi.org/10.1017/jfm.2017.449 Published online by Cambridge University Press

REPETTO, R., SIGGERS, J. H. & STOCCHINO, A. 2010 Mathematical model of flow in the vitreous humor induced by saccadic eye rotations: effect of geometry. *Biomech. Model. Mechanobiol.* **9** (1), 65–76.

REPETTO, R., STOCCHINO, A. & CAFFERATA, C. 2005 Experimental investigation of vitreous humour motion within a human eye model. *Phys. Med. Biol.* **50** (19), 4729–4743.

RILEY, N. 1966 On a sphere oscillating in a viscous fluid. *Q. J. Mech. Appl. Maths* **19** (4), 461–472.

RILEY, N. 1991 Oscillating viscous flows: II superposed oscillations. *Mathematika* **38** (02), 203–216.

RILEY, N. 1998 Acoustic streaming. *Theor. Comput. Fluid Dyn.* **10** (1–4), 349–356.

RILEY, N. 2001 Steady streaming. *Annu. Rev. Fluid Mech.* **33** (1), 43–65.

ROSENBLAT, S. 1959 Torsional oscillations of a plane in a viscous fluid. *J. Fluid Mech.* **6** (02), 206–220.

SADHAL, S. S. 2012*a* Acoustofluidics 13: analysis of acoustic streaming by perturbation methods. *Lab on a Chip* **12** (13), 2292–2300.

SADHAL, S. S. 2012*b* Acoustofluidics 15: streaming with sound waves interacting with solid particles. *Lab on a Chip* **12** (15), 2600–2611.

SADHAL, S. S. 2012*c* Acoustofluidics 16: acoustics streaming near liquid–gas interfaces: drops and bubbles. *Lab on a Chip* **12** (16), 2771–2781.

SADHAL, S. S. 2014 Analysis of acoustic streaming by perturbation methods. In *Microscale Acoustofluidics* (ed. T. Laurell & A. Lenshof), pp. 256–311. Royal Society of Chemistry.

SAURET, A., CÉBRON, D., MORIZE, C. & LE BARS, M. 2010 Experimental and numerical study of mean zonal flows generated by librations of a rotating spherical cavity. *J. Fluid Mech.* **662**, 260–268.

SAURET, A. & LE DIZÈS, S. 2013 Libration-induced mean flow in a spherical shell. *J. Fluid Mech.* **718**, 181–209.

SCHLICHTING, H. 1932 Berechnung ebener periodischer Grenzschichtströmungen. *Phys. Z.* **33** (1932), 327–335.

STOCCHINO, A., REPETTO, R. & CAFFERATA, C. 2007 Eye rotation induced dynamics of a newtonian fluid within the vitreous cavity: the effect of the chamber shape. *Phys. Med. Biol.* **52** (7), 2021–2034.

WANG, C., RALLABANDI, B. & HILGENFELDT, S. 2013 Frequency dependence and frequency control of microbubble streaming flows. *Phys. Fluids* **25** (2), 022002.

WIKLUND, M. 2012 Acoustofluidics 12: biocompatibility and cell viability in microfluidic acoustic resonators. *Lab on a Chip* **12** (11), 2018–2028.

WIKLUND, M., GREEN, R. & OHLIN, M. 2012 Acoustofluidics 14: applications of acoustic streaming in microfluidic devices. *Lab on a Chip* **12** (14), 2438–2451.

ZAPRYANOV, Z. & CHERVENIVANOVA, E. 1981 The flow field induced by the torsional oscillations of a spherical cell containing a fluid drop. *Intl J. Multiphase Flow* **7** (3), 261–270.

ZHANG, K., CHAN, K. H., LIAO, X. & AURNOU, J. M. 2013 The non-resonant response of fluid in a rapidly rotating sphere undergoing longitudinal libration. *J. Fluid Mech.* **720**, 212–235.

ZHAO, H., SADHAL, S. S. & TRINH, E. H. 1999*a* Internal circulation in a drop in an acoustic field. *J. Acoust. Soc. Am.* **106** (6), 3289–3295.

ZHAO, H., SADHAL, S. S. & TRINH, E. H. 1999*b* Singular perturbation analysis of an acoustically levitated sphere: flow about the velocity node. *J. Acoust. Soc. Am.* **106** (2), 589–595.

https://doi.org/10.1017/jfm.2017.449 Published online by Cambridge University Press